AD-A247 532

TION PAGE

Page 1 hour per response, including the time for reviewing instructions, searching existing data sources, gathering and maintaining the collection of information. Send comments regarding this burden estimate or any other aspect of this collection of information, including suggestions for reducing this burden, to Washington Headquarters Services, Directorate for Information Operations and Reports, 1215 Jefferson Davis Highway, Suite 1204, Arlington, VA 22202-4302, and to the Office of Management and Budget, Paperwork Reduction Project (0704-0188), Washington, DC 20503.

1. AGENCY USE ONLY (Leave blank)	2. REPORT DATE 27 February 1992	3. REPORT TYPE AND DATES COVERED Final Technical Report 1 Jan 1990-31 Dec 1991

4. TITLE AND SUBTITLE	5. FUNDING NUMBERS
Study of the Leading-Edge Vortex Dynamics in the Unsteady Flow Over an Airfoil	G. AFOSR-90-0131 2307/CS

6. AUTHOR(S)

B.R. Ramaprain

7. PERFORMING ORGANIZATION NAME(S) AND ADDRESS(ES) Washington State University Pullman, WA 99164-2920	8. PERFORMING ORGANIZATION REPORT NUMBER AFOSR-TR 2 2

9. SPONSORING/MONITORING AGENCY NAME(S) AND ADDRESS(ES) AFOSR/NA Building 410 Bolling AFB, DC 20332-6448	10. SPONSORING/MONITORING AGENCY REPORT NUMBER AFOSR-90-0131

11. SUPPLEMENTARY NOTES

12a. DISTRIBUTION/AVAILABILITY STATEMENT	12b. DISTRIBUTION CODE

13. ABSTRACT (Maximum 200 words)

The two-year project to study the dynamics of the leading-edge vortex (LEV) over a pitching airfoil under conditions of dynamic stall, was started in January 1990. Several accomplishments have been made during these two years. The most significant of these are (i) the construction of a special water channel suitable for the study of dynamic stall over a pitching airfoil, (ii) the measurement of surface pressure distributions over the airfoil under several key operating conditions, and (iii) development of the technique of Particle Image Velocimetry (PIV) and its use in the measurement of the instantaneous velocity and vorticity field in the two-dimensional flow around the airfoil. Some of these data which are the first of their kind have been used to understand the physics of unsteady vorticity dynamics over a pitching airfoil. These data are being made available to other investigators for use as database in validating their numerical models.

14. SUBJECT TERMS Unsteady Aerodynamics, Dynamic Stall, Supermaneuverability, Vortex Dynamics			15. NUMBER OF PAGES 52
			16. PRICE CODE

17. SECURITY CLASSIFICATION OF REPORT Unclassified	18. SECURITY CLASSIFICATION OF THIS PAGE Unclassified	19. SECURITY CLASSIFICATION OF ABSTRACT Unclassified	20. LIMITATION OF ABSTRACT UL

GENERAL INSTRUCTIONS FOR COMPLETING SF 298

The Report Documentation Page (RDP) is used in announcing and cataloging reports. It is important that this information be consistent with the rest of the report, particularly the cover and title page. Instructions for filling in each block of the form follow. It is important to *stay within the lines* to meet *optical scanning requirements*.

Block 1. Agency Use Only (Leave blank).

Block 2. Report Date. Full publication date including day, month, and year, if available (e.g. 1 Jan 88). Must cite at least the year.

Block 3. Type of Report and Dates Covered. State whether report is interim, final, etc. If applicable, enter inclusive report dates (e.g. 10 Jun 87 - 30 Jun 88).

Block 4. Title and Subtitle. A title is taken from the part of the report that provides the most meaningful and complete information. When a report is prepared in more than one volume, repeat the primary title, add volume number, and include subtitle for the specific volume. On classified documents enter the title classification in parentheses.

Block 5. Funding Numbers. To include contract and grant numbers; may include program element number(s), project number(s), task number(s), and work unit number(s). Use the following labels:

C	-	Contract	PR	-	Project
G	-	Grant	TA	-	Task
PE	-	Program Element	WU	-	Work Unit Accession No.

Block 6. Author(s). Name(s) of person(s) responsible for writing the report, performing the research, or credited with the content of the report. If editor or compiler, this should follow the name(s).

Block 7. Performing Organization Name(s) and Address(es). Self-explanatory.

Block 8. Performing Organization Report Number. Enter the unique alphanumeric report number(s) assigned by the organization performing the report.

Block 9. Sponsoring/Monitoring Agency Name(s) and Address(es). Self-explanatory.

Block 10. Sponsoring/Monitoring Agency Report Number. *(If known)*

Block 11. Supplementary Notes. Enter information not included elsewhere such as: Prepared in cooperation with...; Trans. of...; To be published in.... When a report is revised, include a statement whether the new report supersedes or supplements the older report.

Block 12a. Distribution/Availability Statement. Denotes public availability or limitations. Cite any availability to the public. Enter additional limitations or special markings in all capitals (e.g. NOFORN, REL, ITAR).

DOD	-	See DoDD 5230.24, "Distribution Statements on Technical Documents."
DOE	-	See authorities.
NASA	-	See Handbook NHB 2200.2.
NTIS	-	Leave blank.

Block 12b. Distribution Code.

DOD	-	Leave blank.
DOE	-	Enter DOE distribution categories from the Standard Distribution for Unclassified Scientific and Technical Reports.
NASA	-	Leave blank.
NTIS	-	Leave blank.

Block 13. Abstract. Include a brief (*Maximum 200 words*) factual summary of the most significant information contained in the report.

Block 14. Subject Terms. Keywords or phrases identifying major subjects in the report.

Block 15. Number of Pages. Enter the total number of pages.

Block 16. Price Code. Enter appropriate price code (*NTIS only*).

Blocks 17. - 19. Security Classifications. Self-explanatory. Enter U.S. Security Classification in accordance with U.S. Security Regulations (i.e., UNCLASSIFIED). If form contains classified information, stamp classification on the top and bottom of the page.

Block 20. Limitation of Abstract. This block must be completed to assign a limitation to the abstract. Enter either UL (unlimited) or SAR (same as report). An entry in this block is necessary if the abstract is to be limited. If blank, the abstract is assumed to be unlimited.

Table of Contents

A-1

List of Figures

STUDY OF THE LEADING-EDGE VORTEX DYNAMICS
IN THE UNSTEADY FLOW OVER AN AIRFOIL

B.R. Ramaprian

Principal Investigator

A. ABSTRACT

The two-year project to study the dynamics of the leading edge vortex (LEV) over a pitching airfoil under conditions of dynamic stall, was started in January 1990. Several accomplishments have been made during these two years. The most significant of these are (i) the construction of a special water channel suitable for the study of dynamic stall over a pitching airfoil, (ii) the measurement of surface pressure distributions over the airfoil under several key operating conditions, and (iii) development of the technique of Particle Image Velocimetry (PIV) and its use in the measurement of the instantaneous velocity and vorticity field in the two-dimensional flow around the airfoil. Some of these data which are the first of their kind have been used to understand the physics of unsteady vorticity dynamics over a pitching airfoil. These data are being made available to other investigators for use as database in validating their numerical models. This Final Technical Report describes briefly the various accomplishments mentioned above. More detailed descriptions can be found in several forthcoming reports/publications. Further analysis of the experimental data obtained so far, and the extension of the studies to three-dimensional unsteady flow fields has started under a new AFOSR Grant which was initiated on February 15 1992.

B. BRIEF OUTLINE OF RESEARCH ACCOMPLISHMENTS

I. Introduction

This project was started on January 1, 1990. The main objective of this project is to understand the basic physics of the production, diffusion and convection of the leading-

edge vortex (LEV) and the role of the LEV in the onset of dynamic stall over an airfoil subjected to rapid pitching. The study is relevant to aircraft supermaneuverability. The project involved conducting a comprehensive set of experiments in a specially designed hydraulic facility, from which information on pressure, velocity and vorticity fields associated with the LEV and dynamic stall over a pitching airfoil was obtained. The pressure measurements were made using pressure transducers, while the velocity measurements (and hence the vorticity measurements) were obtained using PIV. The research effort under this Project is being closely co-ordinated with that under an other project on the study of the dynamic stall process in three-dimensional flow over wings, supported by the U.S. Army Research Office. The accomplishments during the two-year project period are briefly described below.

II. Construction of Water Channel and Airfoil

A 1 m × 0.7 m, free-surface, water channel suitable for the study of dynamic stall has been constructed. It has a 4 m long test section. The channel is constructed of PVC and stainless steel to prevent rust formation. The water quality is carefully controlled by a combination of softening, filtering, chlorination and pH management. The flow in the test section is uniform to within 1%, and has a freestream turbulence level of under 1%. The test section velocity can be varied from 0 - 1.7 ft/s. The channel is fully seeded with 2-micron size fluorescent particles to allow the use of PIV. The facility, which can be used for the study of dynamic stall over airfoils, represents the state of the art in terms of the quality of flow.

The test model is a NACA 0015 airfoil of 35-cm chord (c) and 70-cm span, formed from extruded aluminum stock, and painted dull black to prevent glare and reflection during flow visualization and PIV measurements. It is provided with 41 surface pressure taps on one side. The fine distribution of the pressure taps allows the measurement of pressures at intervals of about $0.01c$ in the nose region. The airfoil is suspended in water with its span vertical. It is provided with a circular transparent end plate which just dips into the water. The end plate serves to prevent wave effects at the free surface. It also provides an unobstructed and distortion-free view of the flow field around the airfoil. The end plate is carried by a large (65-cm diameter) bearing and can be rotated clockwise or counterclockwise over an angle of

80 degrees, via a chain drive, by a computer-controlled stepper motor. Since the airfoil is mounted with its $c/4$-axis passing through the center of the end plate, the rotation of the end plate causes the airfoil to be pitched about this axis, with the angle of incidence (α) varying in the range of -40 to +40 degrees. The airfoil support system is also designed to be capable of translating the airfoil along the channel at any desired acceleration. The linear motion is provided by a feed-back controlled brushless D.C. motor. Schematics of the water channel and the airfoil assembly are shown in Figs. 1 and 2. More details of the flow facility and the model will be provided in a forthcoming report.

III. Pressure Measurements

1. Instrumentation and Experimental Procedure

Surface pressures on the airfoil were measured using a diaphragm-type pressure transducer mounted outside the airfoil on the end plate and connected to the pressure taps by approximately 35 cm of 3 mm stainless tubing and 15 cm of 6 mm Tygon tubing. A scanning valve was used to switch the pressure transducer between the pressure taps. The transducer output was sampled, digitized, acquired and stored by a personal computer. An encoder mounted on the pitching motor shaft, and an electronic counter allowed the data to be sampled at 3000 equal angular intervals during the pitching period. The phase-locked pressure vs time history was thus obtained for several pitching realizations, from which "ensemble-averaged" values could be evaluated. This information was then corrected for possible inadequate dynamic response of the pressure measurement system, and subsequently processed to obtain the instantaneous chordwise pressure distribution over the airfoil at any desired incidence. These distributions were then integrated to obtain the instantaneous lift, pressure drag and pitching moment coefficients C_l, C_d and $C_{m,c/4}$, as functions of the incidence angle α.

The measurement of unsteady pressures in water posed a significant challenge, especially since no similar previous effort had been documented. Details of the measurement procedure

(including studies of dynamic response of the measurement system) will be given in two forthcoming reports.

Tests were performed at three different (nominal) Reynolds numbers; 0.5×10^5, 1.3×10^5, 2.2×10^5, and at nondimensional pitch rates α^+ defined by

$$\alpha^+ = \frac{c\dot{\alpha}}{U_\infty}$$

ranging from 0.036 to 0.2. This range includes the value of 0.072 studied by Acharya and Metwally at IIT, Chicago, in their experiments in a wind tunnel at a Reynolds number of about 1.0×10^5 using a NACA 0012 airfoil.

2. Summary of Results

The main results of the experiments are summarized below. Pressure data are shown in terms of C_p defined in the usual manner.

2.1. Pressure-Time History

Typical variations of C_p with the angle of incidence α during the pitching process are shown in Fig.3 for several chordwise locations. This figure corresponds to a Reynolds number of 1.3×10^5 and a nondimensional pitching rate of 0.1. The evolutions of C_p at other Reynolds numbers and pitching rates are qualitatively similar to those shown in this figure. The initial increase in the magnitude of the negative C_p near the nose region is a result of the generation of strong clockwise vorticity at the surface near the leading edge. This process reaches a maximum at $\alpha \approx 20 - 30$ degrees, the exact angle depending on the Reynolds number and pitching rate. Comparison with the velocity field around the airfoil (to be discussed later) showed that the leading-edge-vortex begins to form slightly before this maximum C_p is attained. The subsequent rapid decrease in the suction pressure is correlated with the shedding of the LEV from the airfoil.

At a more downstream point, there is no substantial generation of clockwise vorticity locally. In fact, there may be a significant amount of counterclockwise vorticity generation

at these locations because of the local adverse pressure gradient. Clockwise vorticity appears at these locations essentially because of convection from the upstream regions. The suction peak, which correlates with the strength of clockwise vorticity, therefore, appears later in the pitching cycle compared to the leading-edge region. For the same reason, the suction peaks at successive downstream locations shift to larger and larger incidences. This vorticity is usually (but not necessarily) carried by the LEV. At any given location, the suction peak breaks down when the LEV leaves the surface, carrying with it the clockwise vorticity. The above statements apply to all the points along the airfoil. However, the region near the trailing edge does not show spectacular variations in pressure history. Likewise, the pressure side of the airfoil also does not exhibit any noteworthy features in its pressure history.

The present results are qualitatively similar to the previous results reported in the literature. There are, however, significant quantitative differences. The magnitudes of the highest suction peaks measured in the present experiments (which increase from about 10 at $Re = 5 \times 10^1$ to about 17 at $Re = 2.2 \times 10^5$) are much higher than the values of 4 or 5 measured at a Reynolds number of about 1×10^5 in the wind tunnel experiments of Acharya and Metawally (1990). They are, however, of the same order as those measured at very high Reynolds numbers by Lorber and Carta (1987). There thus appears to be a very rapid approach to high-Reynolds number flow conditions in the water channel. Several basic tests were performed to understand this trend. These will be described in detail in the forthcoming report referred to earlier..

2.2. Reynolds Number Effects

Figures 4-6 show typical C_p vs x/c plots at three different Reynolds numbers. In all these cases, the pitching rate $\alpha^+ = 0.072$. From the examination of these plots, it is possible to make some observations about the flow behavior. The first noticeable characteristic is an initial suction peak located at about 1% of the chord length from the nose, on the suction side of the airfoil. The magnitude of this peak is initially small, but continually increases until about $\alpha = 21\text{-}24$ degrees, the exact angle depending upon the Reynolds number. Simultaneously, the suction peak moves towards the nose. After reaching this maximum value, the peak

suddenly collapses. This initial peak and its movement towards the nose as α increases, are well documented in similar experimental (Acharya and Metwally 1990) and numerical (Visbal 1991) studies of these flows. The present experiments however, yield C_p values of much higher magnitude than previous studies, as already mentioned. As this peak begins to collapse, a second peak simultaneously grows at an x/c position of approximately 0.2. This secondary peak continues to grow for another 3-4 degrees before slowly leveling off. The second peak is more clearly observable at the higher Reynolds numbers (Figs.5b,6b). Study of the velocity field around the airfoil seems to indicate that the secondary peak appears approximately around the time the shear layer separates from the airfoil surface near the leading edge.

While the peak magnitudes and phase relations of C_p are seen to vary noticeably with Reynolds number, the Reynolds-number dependence is much less apparent in the force and moment coefficients evaluated from the measured C_p distributions. This is typically seen in the plots of C_l, C_d and $C_{m,c/4}$ vs.α shown in Figs.7(a)-7(c) for the three Reynolds numbers. For all the three cases, the lift seems to increase nearly linearly from 0 to 23 degrees. In fact, the present results collapse over each other and, for $0 < \alpha < 21$ degrees, over the earlier results, as well. The difference, however, is that the increase seems to continue up to about 27 or 28 degrees, which is well beyond the value observed in other experiments at similar Reynolds numbers and α^+ values. Beyond $\alpha \approx 28$ degrees, C_l begins to decrease, and the lift curves at different Reynolds numbers begin to deviate from each other. The drag and the pitching-moment coefficients exhibit a similar behavior with respect to Reynolds-number dependence.

Figures 8(a) - *(c) show the distribution of the pressure gradient $\frac{dC_p}{d(s/c)}$, (where s is the coordinate along the airfoil surface) at $\alpha \approx 15, 20$ and 25 degrees at the two lower Reynolds numbers, and at $\alpha \approx 20, 25$ and 30 degrees at the highest Reynolds number studied. These angles have been chosen so as to show the rise and fall of the maximum negative pressure gradient in the flow. The very large magnitudes at or very close to the nose, which are similar to those reported by Acharya and Metwally (1990), indicate large infusion of lift-producing clockwise vorticity into the flow within a very short region from the nose. As would be expected, these distributions exhibit higher magnitudes at higher Reynolds numbers. At any given Reynolds number, the magnitude of the negative gradient increases towards the incidence corresponding to the maximum suction peak (and hence, to the formation of the LEV). The

PIV data obtained so far seem to suggest that the positive maximum of the gradient seems to correspond to the instant just prior to the separation of the shear layer from the surface. It can be seen that this positive peak increases in magnitude and moves upstream along the suction side of the airfoil, as the Reynolds number increases. In fact, at the highest Reynolds number studied, the positive peak is located at $s/c \approx 0.05$.

2.3. Pitching Rate Effects

Figures 9-12 show the pressure distributions along the airfoil at the same nominal Reynolds number of about 1.3×10^5, but at four different pitch rates, namely $\alpha^+ = 0.036, 0.072, 0.1$ and 0.2. The distributions at the different pitch rates are similar qualitatively. However, it can be seen that as the pitch rate increases, the maximum suction peak increases to very large values ($C_{p,max} \approx -19$). It is also seen that as the pitch rate increases, the suction peak in the pressure distribution occurs at a higher angle of incidence, and the second peak becomes more pronounced. Also, a pressure plateau appears at and around the angle of incidence corresponding to the maximum suction peak. The plateau is more pronounced at the lower pitching rates.

The effect of pitching rate on the force and moment coefficients are shown in Figs.13(a)-13(c). Once again, for the sake of brevity, the results for C_l only will be discussed here. The other coefficients behave in a similar manner. It is seen that at lower pitch rates, the lift curves essentially coincide with the steady-state curve in the prestall regime. In fact, the effect of unsteadiness at these pitch rates seems to be merely to extend the steady-state curve to higher angles of incidence. As the pitch rate increases, however, the lift increases above the steady-state value at all incidences. In fact, there is a noticeable amount of lift even near zero incidence, at the higher pitch rates. This is due to the significant "virtual mass effect" associated with the wall motion. Also, the present experiments indicate that, at the highest pitch rate, the lift continues to increase up to an incidence of 35 degrees, even though the results at these high incidence angles, are not very reliable due to blockage and possible three-dimensional effects.

All the lift curves indicate some oscillation near zero incidence. This is presently suspected

to be due to the effect of initial acceleration on the pressure tubings. Also, a certain waviness can be noticed in the lift curves. This feature has been observed also in the available data from wind tunnels. We have no explanation, at this time, for this behavior.

III. Velocity Measurements using PIV

1. *Background*

While there have been several flow visualization studies and pressure/force measurements of pitching and oscillating airfoils, no detailed experimental data on the flow field around the airfoil are available. The data on velocity and vorticity distribution in the flow field are crucial for the understanding of the vorticity dynamics associated with lift augmentation and dynamic stall. To the best of our knowledge, there is only one other PIV study of this flow, apart from the present experiments, that has been reported in the literature (Shih et. al. 1990). The features that distinguish the present experiments are: (i) they have been performed on a much larger model, and (ii) the flow field has been subdivided into three regions,- the front, middle and aft,- for detailed study. These features have allowed us to obtain a very much higher degree of spatial and temporal resolution of the flow field, and data relatively much closer to the wall, than has hitherto been possible.

2. *The PIV System*

Considerable effort was devoted during the first year of the Project to the development of the PIV system. During this period, the necessary hardware (including the pulsed laser, image processor, interrogating system and the camera drive), as well as the software for processing the pictures (including interrogation, image acquisition, FFT and post-processing algorithms) were developed. During the course of PIV development, several alternate procedures were

evaluated and the technique best suited for the present study was identified. This system was then fully automated and tested. A schematic of the PIV system is given in Fig.14. The processing speed was vastly improved during the early part of the second year of the Project, by the addition of an array processor. A considerable amount of effort has also been put into the development of post-processing software, such as for the checking and correction of "bad" data, interpolation for missing points, computation of stream function and vorticity, use of variable grid spacing, etc. As a part of the development process, the present system was successfully used for measuring the instantaneous streamlines and vorticity contours in the Kárman vortex street behind a cylinder impulsively started from rest. The development and testing of PIV has formed the subject of two M.S. dissertations and has been submitted for presentation at conferences (see list of publications).

The PIV system was then used for obtaining the instantaneous velocity and vorticity field around the pitching 2-D airfoil in the water channel.

3. *PIV Experiments on the Pitching Airfoil*

The experiments reported here were performed at a Reynolds number of 15,000 and are hence suitable for comparison with the computational results obtained from some of the existing low-Reynolds number codes (e.g. Visbal 1991). The evolution of the flow over the range $0 < \alpha < 30$ degrees was studied. The pitching rate $\dot{\alpha}$ was maintained constant in these experiments at 0.072.

During the PIV experiments, the entire water channel was seeded with fluorescent particles of 2μm diameter. The horizontal midspan plane of the test section on the suction side of the airfoil was illuminated with a thin light sheet from a 5-watt argon laser. The laser light sheet was pulsed at a frequency of 60 Hz by using a rotating shutter in the optical path. Instantaneous multiple-exposure pictures of the illuminated particles were taken through the transparent end-plate. A Nikon F3 35-mm camera mounted on the end-plate and moving with it, was used for this purpose. Thus, data were obtained in a co-ordinate frame moving with the airfoil. The motor drive on the camera was triggered by a clock to take consecutive pictures at predetermined intervals. The camera shutter and the airfoil motion were also synchronized

by the clock. The multiple-exposed photographs were taken at intervals of about 0.75 degree in pitch over a range of 0-30 degrees. Three separate experiments were performed during which the camera was "zoomed in" on the forward, middle and aft regions of the flow field respectively.

Each photographic film was analyzed statistically to obtain the instantaneous velocity field. For this purpose, the film was divided into 100 segments. Each segment was digitized using a microscope objective, a CCD camera and a digital image processor. This digitized image was further divided into 16 subsegments. The mean velocity vector over each subsegment was obtained by computing the two-dimensional autocorrelation function of the digitized image, using a high-speed array processor. The film was scanned using a two-dimensional traverse, to obtain the velocity vectors over the entire flow field. Instantaneous vorticity field and streamlines were then computed from the measured velocity vector field. The entire procedure has been automated. The flow field has been resolved to $0.008c \times 0.008c$ in space, and 0.002 of the pitching period in time.

4. Results of PIV Experiment

4.1. Velocity Vectors and Vorticity Contours

Typical sets of results for the nose region of the airfoil are shown in Figures 15 and 16. Figure 15 shows the velocity fields and Fig. 16 the vorticity contours. These figures cover a range of pitch angles from 15.3 to 22.5 degrees. It is seen from Fig. 15 that clockwise vorticity contours start "bulging" outwards at $\alpha = 15.3$ degrees around $x/c = 0.15$. This process continues till at $\alpha = 16.9$ degrees, the vorticity contours appear to close, indicating the formation of the first vortex structure near the leading edge. Results at $\alpha = 19.3$ degrees indicate more vortices but no significant lateral growth in the vortical region. At $\alpha = 22.5$ degrees, the flow is characterized by a large number of alternating clockwise and counterclockwise vortices, that closely resemble shear-layer vortices. In fact, the flow structure during the incidence range

of 17-22.5 degrees appears like a detaching (separating) shear layer, except that the vortices resulting from the shear-layer instability remain quite close to the surface,- within a distance of about 0.15c. Note that even at 22.5 degrees, strong vorticity contours still lie close to the wall, even though reverse flow appears to extend much farther. This is presumably due to the effect of the wall motion. The presence of strong vorticity close to the wall explains why lift continues to increase beyond the static-stall incidence. The vortex structure at 22.5 degrees has, however, all the attributes of the dynamic stall vortex.

More details of the flow can be seen from Figs.17-19 which show the velocity vectors and vorticity contours over the front, mid and aft regions of the airfoil at three incidences, namely 15.3, 20.1 and 23.4 degrees respectively. In addition, the details of flow in the aft region are shown in Fig.20 for the incidence of 8.9 degrees. It is seen that at 15 3 degrees, the vorticity contours near the leading edge are still parallel and concentrated at the surface. There is no evidence of any vortex generation in this region at this incidence. However, one can see in Fig.20, the presence of a thin layer of flow reversal near the trailing edge at an angle of 8.9 degrees. It seems that this thin reverse-flow region evolves and the clockwise vorticity associated with it creeps upstream towards the leading edge and initiates the development of the LEV at an angle of about 16 degrees. The counterclockwise vorticity and the reverse flow seen in the midregion at 15.3-degree incidence in Fig.17(a) are due to the trailing-edge vortex creeping upstream along the airfoil. These results thus seem to support the mechanism suggested by the numerical calculations of Visbal (1991).

At 20.1-degree incidence, the shear layer near the leading edge has separated from the surface at $x/c \approx 0.125$ (Fig.18a). The instability of this shear layer has resulted in distinct vortices the first of which we designate as the LEV. A part of this vortex structure is seen over the midregion in Fig.18(b). It is interesting to note that at this angle, the shear layer and the vorticity is still located close to the surface. This is the reason for the continued increase in lift at this angle. Note that at this angle, the vorticity information from the upstream region has not yet reached the aft region of the airfoil (Fig.18c).

Figure 19(a) shows that at the incidence of 23.4 degrees, the shear layer has clearly detached itself from the surface and the point of separation has also moved upstream towards the leading edge ($x/c \approx 0.05$). The vortices have coalesced into a large vortex (the so-called dynamic stall vortex) which can be seen over the midregion of the airfoil in Fig.19(b).

Figure 19(c) shows a part of a large clockwise vortex in its northwest corner. We believe that this is a part of the dynamic stall vortex convected from the midregion during this 'tching realization. Apparently, during this particular realization, the vortex has advanced a little faster than in the realization shown in Fig.19(b). The unsteady flow over the pitching airfoil is significantly influenced by the shear-layer instability and the resulting vortex-vortex interactions. We, therefore, believe that the flow pattern is not strictly deterministic. It may, therefore, not always possible to see continuity in the flow pattern between two regions of the flow, if these are visualized during different pitching realizations. This is particularly true for the mid and aft regions, after detachment of the shear layer from the airfoil surface.

Figures 21, 22 and 23 show the distributions of the U_s and U_n components of the velocity at three longitudinal locations, $s/c = 0.173, 0.375$ and 0.827, as typical examples of the quantitative information obtained from the present experiment, that can be used by computors, for comparison with the results of their numerical computations. These distributions are shown in curvilinear coordinates with s along and n normal to the airfoil surface. These results have been obtained from co-ordinate transformation (and interpolation) of the PIV data obtained in a rectangular coordinate system fixed to the airfoil. The sharp changes in the velocities indicate the presence of vortices. The jaggedness of the data is a measure of the random measurement errors, as well as the inherent limitation of the spatial and temporal resolution of the PIV system. The figures show that the present measurements provide an acceptable data base for verification and validation of numerical computations. In fact, the present data are being made available to Professor Ghia at the University of Cincinnati for comparison with his numerical computations.

4.2. Analysis of Vortex Dynamics

Some preliminary analysis of the vortex dynamics of the flow has been made along the lines suggested in the original proposal of this Project. As a first step, the location of the center of the LEV vortex at each instant after its formation was computed from the definitions

$$x_c = \frac{\int \int_R x \omega_z \, dx \, dy}{\int \int_R \omega_z \, dx \, dy}$$

and

$$y_c = \frac{\int\int_R y\omega_z\,dx\,dy}{\int\int_R \omega_z\,dx\,dy}$$

where R the region of integration was inferred visually from the vorticity contours obtained from PIV. Figure 24(a) shows the coordinates x_c and y_c as a function of α, during the pitching process,. Figure 24(b) shows the trajectory of this vortex during pitching. The points shown in these figures correspond to the situations in which the vortex was either in the front or mid region of the flow. Situations in which the vortex was in the aft region have not been included because of the difficulty encountered in matching different realizations. In any case, these situations correspond to post-dynamic-stall incidences and hence, are not of much interest to this study. It is seen that LEV forms at the point with the approximate co-ordinates $x_c = 0.2c, y_c = 0.09c$, (i.e. at a distance of about $0.05c$ from the surface) at an incidence of about 16 degrees. It moves momentarily a short distance upstream before being washed downstream and away from the surface. The trajectory of the vortex center is initially curved, but soon becomes nearly a straight line. The effective terminal convection velocity of the vortex relative to the airfoil along the chordwise direction is about $0.12U_\infty$.

The circulation Γ_V associated with this vortex was estimated from

$$\Gamma_V = \int\int_R \omega_z\,dx\,dy$$

The results are shown in Fig.25. In this figure, Γ_V is normalized by $(\alpha\pi U_\infty c)$ which is the magnitude of the circulation associated with the bound vortex around the airfoil (calculated from thin-airfoil theory). It is seen that the vortex gains strength rapidly after its formation. This is due to the infusion of vorticity into the vortex resulting from the coalescence of the shear layer vortices, which are continuously fed with vorticity from the favorable pressure gradient at the upstream regions of the pitching airfoil surface. The vortex circulation could not be calculated beyond 28 degrees of incidence, because of the matching difficulties stated earlier. It is seen that the circulation associated with the dynamic-stall vortex eventually reaches a value as high as 70% of the total bound-vortex circulation around the airfoil prior to the occurrence of dynamic stall.

Based on a model suggested by Reynolds and Carr (1985), it was hypothesized in the original proposal of this Project that the first appearance of the LEV should correspond to the condition that the downstream velocity of the center of the vortex U_c should be equal to the

upstream velocity induced at the center of the vortex by its image in the airfoil. The induced velocity U_i can be obtaibed from

$$U_i = \frac{\Gamma_V}{4\pi N_c}.$$

where $N - c$ is the normal distance of the center of the vortex from the airfoil surface. Figure 26 shows the values of U_c and $-U_i$ plotted as a function of α. While these data somewhat seem to suggest that the LEV formation occurs for $\alpha \approx 18$ degrees. the scatter in the data is too large to allow us to make any definitive statement, at this time, about the success of the model. More study of the data is in progress.

IV. Active Control of LEV Dynamics

Some effort was devoted, under partial support from this Grant, to the study of the possibility of actively controlling the dynamics of the LEV and hence the unsteady lift. This work was performed at the Siler laboratory, Airforce Academy, Colorado Springs, by Ms. Julie Lavato as part of her Ph.D. Dissertation, which was completed and submitted to Washington State University in February 1992. Ms. Lavato was supported by the present Grant during the period December 1, 1990 through May 15, 1991. Her work at Siler Laboratory involved the study of the structure of the shear layer and the associated vortices formed during the pitch-up motion of a NACA 0015 airfoil at low Reynolds numbers in a wind tunnel, and the effect of external forcing on this structure. The external forcing included both acoustic excitation from a speaker and periodic pulsing of an air jet through a tangential slot near the leading edge. Her experiments showed that the shear layer strongly responds to forcing frequencies that are subharmonics of the fundamental frequency of the shear-layer vortices. They further showed, that if the flow is forced at the appropriate frequency, a delay of 3-4 degrees in dynamic stall, and up to 25% increase in lift can be obtained over a pitching airfoil at $\alpha^+ = 0.05$. The studies and the results obtained are described in detail in the Ph.D. thesis of Lavato (Lavato 1992). This work greatly complements the PIV studies at WSU, that have identified the dominant presence of the shear layer vortices in the flow over a pitching airfoil.

V. Related Studies on 3-D Flows

As already stated, the experiments on the two-dimensional pitching airfoil are being co-ordinated with simultaneous experiments on a finite aspect-ratio rectangular wing of NACA 0015 profile. The latter studies supported by ARO, are being performed in a wind tunnel using three-component fiber-optic based Laser Doppler Velocimetry (LDV). During the past two years, velocity and vorticity measurements have been made in the 3-D flow field of the tip vortex (WTV) behind the wing. These data have been obtained both when the wing is stationary, and when it is oscillated sinusoidally in pitch about its c/4 axis. These are probably the first detailed data of their kind on the WTV. This work formed the Ph.D. thesis of Mr. Y.Zheng. The thesis is presently being written while part of the results from the studies have already been published (see list of publications). Apart from the fact that the 3-D data will complement the 2-D data from the water channel studies, the ARO project has also resulted in the development of a significant amount of data acquisition and processing software required for the phase-locked measurements in the water-channel experiments.

VI. CONCLUDING REMARKS

The two year-research effort has made the following important contributions:

1. A comprehensive data base has been generated on the unsteady pressure distribution over a pitching airfoil at low Reynolds numbers and low to moderate pitching rates. The large length and time scales in the water channel experiments have allowed us to obtain spatial and temporal resolutions that are difficult, if not impossible, to attain in conventional wind-tunnel experiments.

2. A very detailed set of velocity and vorticity measurements has been obtained in the flow around the pitching airfoil at a Reynolds number of 15,000. Once again, the large length and time scales in the water channel have been exploited to obtain higher spatial and temporal resolutions than have been achieved in the past. It has been therefore, possible, to study in great detail, several aspects of the flow, such as the formation of the LEV in the nose region, the growth and instability of the shear layer,

and the growth and convection of the LEV. The PIV data have, in fact, been used in a preliminary way, for the verification of an LEV model suggested in the original proposal of this project.

3. An important observation from these studies is that shear-layer separation and its instability resulting in the formation of vortices is an important aspect of the unsteady flow dynamics over the pitching airfoil. This has two important implications:

   a. Since shear-layers are sensitive to external forcing, it should be possible, in principle, to control the flow dynamics by means of active control techniques that can alter this shear-layer behavior. In fact, the work at Siler Laboratory has demonstrated the feasibility of this concept.

   b. Since the vortex structure resulting from shear-layer instability can vary in detail from one pitching realization to another, it is doubtful whether an individual realization can be correctly predicted even in laminar flow, by any numerical technique, without knowing the exact initial conditions. However, since the shear-layer dynamics is still driven, in a stochastic sense, by the pitching process, prediction of the flow should still be possible on an *ensemble-average* basis. One should, therefore, look for broad, rather than, detailed agreement while using experimental data from a single realization for comparison against numerical predictions.

In addition to the above, the Project has resulted in the development of a state-of-the-art flow facility and PIV/LDV capability that can be used in further studies of vortex dynamics in two and three-dimensional unsteady flows. The data that have been obtained so far, along with some additional data to be obtained in the coming months under the new AFOSR Grant, will be used to further examine the dynamics of the LEV.

VII. References

Acharya, M., and Metwally, M.H. 1990 "Evolution of the Unsteady Pressure Field and Vorticity Production at the Surface of a Pitching Airfoil'" AIAA Paper No.90-1472.

Lorber,P.F., and Carta, F.O. 1987 "Unsteady Stall Penetration Experiments at High Reynolds Numbers," UTRC Report R87-956939 (AFOSR TR-87-1202), United Technologies Re-

search Center, East hartford, CT.

Reynolds, W.C., and Carr, L.W. 1985 "Review of Unsteady Driven Separated Flows," AIAA Paper No. 85-0527.

Shih, C., Lourenco, L., Van Dommelen, L., and Krothapalli, A. 1990 "Unsteady Flow Past an Airfoil Pitched at Constant Rate," Proc. of the Int. Symp.on Nonsteady Fluid Dynamics, ASME FED, Toronto, June 4-7, pp.41-50.

Visbal, M.R. 1991 "On the Formation and Control of the Dynamic Stall Vortex on a Pitching Airfoil," AIAA Paper No. 91-0006.

C. PERSONNEL, DEGREES AWARDED AND PUBLICATIONS

I. Personnel and Degrees Awarded

B.R. Ramaprian	PI	
Rand Conger	Graduate Research Assistant	M.S. student (Completing in Spring 1992)
Hideya Oshima	Graduate Research Assistant	M.S. awarded in Dec 90
Julie Lovato	Graduate Research Assistant	Ph.D. student (completing in Spring 1
Youxin Zheng	Graduate Research Assistant	Ph.D. student (completing in June 1992)
Tim Falk	Off-Campus Graduate student	M.S. awarded in June 90

II. Manuscripts Submitted or Published

1. Publications

Oshima, H., and Ramaprian, B.R., "The Use of Particle Image Velocimetry to Study Vortex Shedding Behind A Cylinder," Proc. of The Forum on Fluid Measurements and Instrumentation, *First ASME/JSME Fluids Engrg. Conference*, Portland, OR, June 23–27, 1991., pp.15-20

Zheng, Y., and Ramaprian, B.R., "LDV Measurements in the Roll-Up Region of the Tip Vortex from a Rectangular Wing," AIAA Paper No. 91-1685, Presented at the *AIAA 22nd Fluid Dynamics, Plasma Dynamics and Lasers Conference*, Honolulu, HY, June 24–26, 1991,

Zheng, Y., and Ramaprian, B.R., "LDV Measurements in the Unsteady Tip-Vortex Behind an Oscillating Rectangular Wing," Proc. of the *Eighth Symposium on Turbulent Shear Flows*, Munich, Germany, Sept. 9–11,1991,

Oshima, H.O., and Ramaprian, B.R., "Measurement of the Velocity and Vorticity Fields around a Pitching Airfoil," AIAA Paper No. 92-2626, to be presented at the *AIAA 10th Applied Aerodynamics Conference*, Palo Alto, CA, June 22-24.

2. Dissertations

Oshima. H., "The Development of Particle Image Velocimetry," M.S. Dissertation, Dept. of Mech. and Materials Engrg., Washington State University, Pullman, WA, December 1990.

Falk, T.L., "Software for Particle Image Velocimetry," M.S. Dissertation, Department of Mechanical Engineering, Washington State University Vancouver Campus, Vancouver, WA, May 1990.

Lavato, J., "Active Control of the Separation Region on A Two-Dimensional Airfoil," Ph.D. Thesis, Mechanical Engineering, Washington State University, Pullman, Wa, February

1992.

Conger, R.C., "Pressure Measurements on a Pitching Airfoil in a Water Channel," M.S. Thesis, Mechanical Engineering, Washington State University, Pullman, WA. March 1992 (to be submitted).

Inlets

Screens

Head Tank

Plastic Honeycomb

Plastic Honeycombs

Pitching Mechanism

Test Section
Width: 0.9 m
Depth: 0.69 m
Length: 3.68 m

Tail Tank

Pump

Pump

Bypass Valves

Top View

Pitching Mechanism Supports

Airfoil

Glass Walls for
Visualization, PIV, LDV

Pumps

Bypass Valves

25.4 cm Pipes

Side View

Fig. 1. Water Channel

123.3 cm

Chain

63.5 cm
o.d.

Motor

118.1
cm

Motor

63.5 cm

29.8 cm

Pressure Taps

60.3 cm

63.5
cm

1.9 cm

89.5 cm

Fig. 2. Airfoil Pitching Mechanism
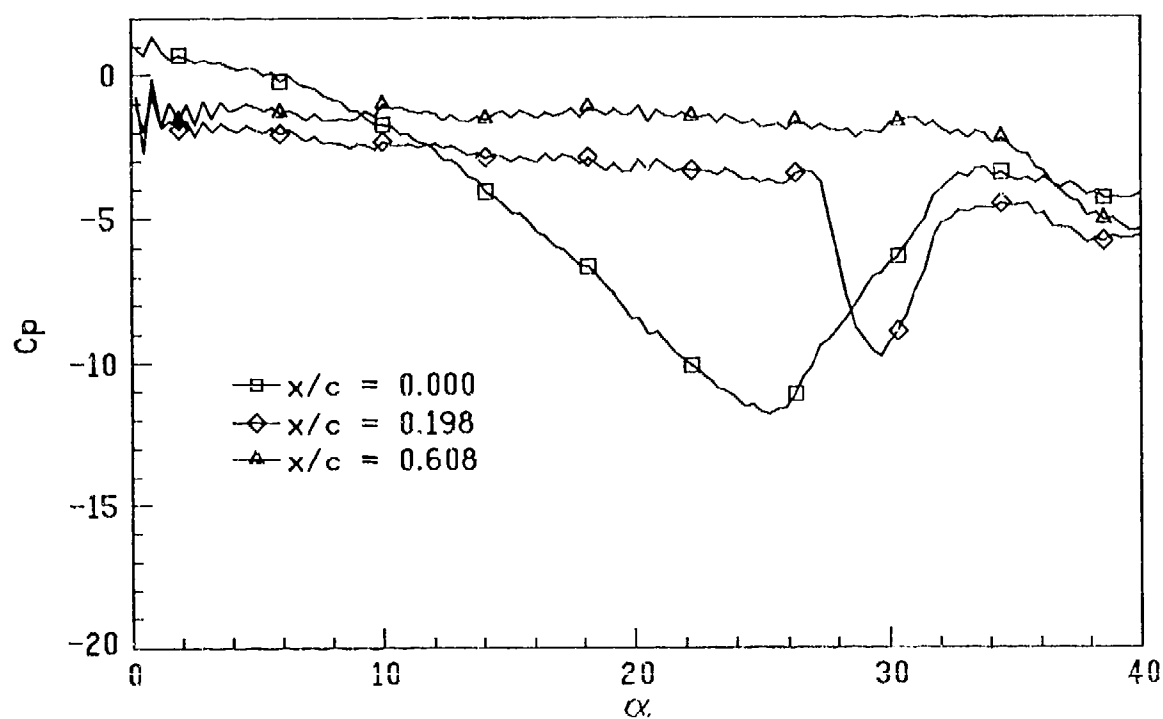
Fig. 3a. C_p vs. α at fixed x/c positions. $Re = 1.3 \times 10^5$; $a^+ = 0.100$
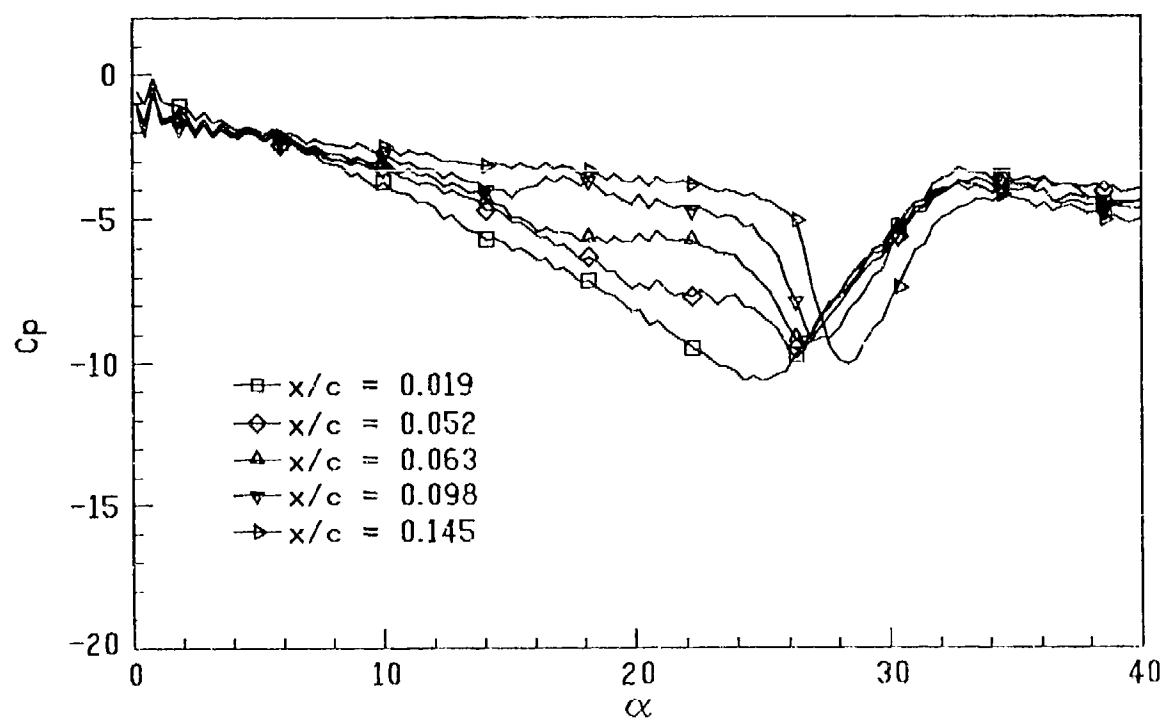
Fig. 3b. C_p vs. α at fixed x/c positions. $Re = 1.3 \times 10^5$; $a^+ = 0.100$
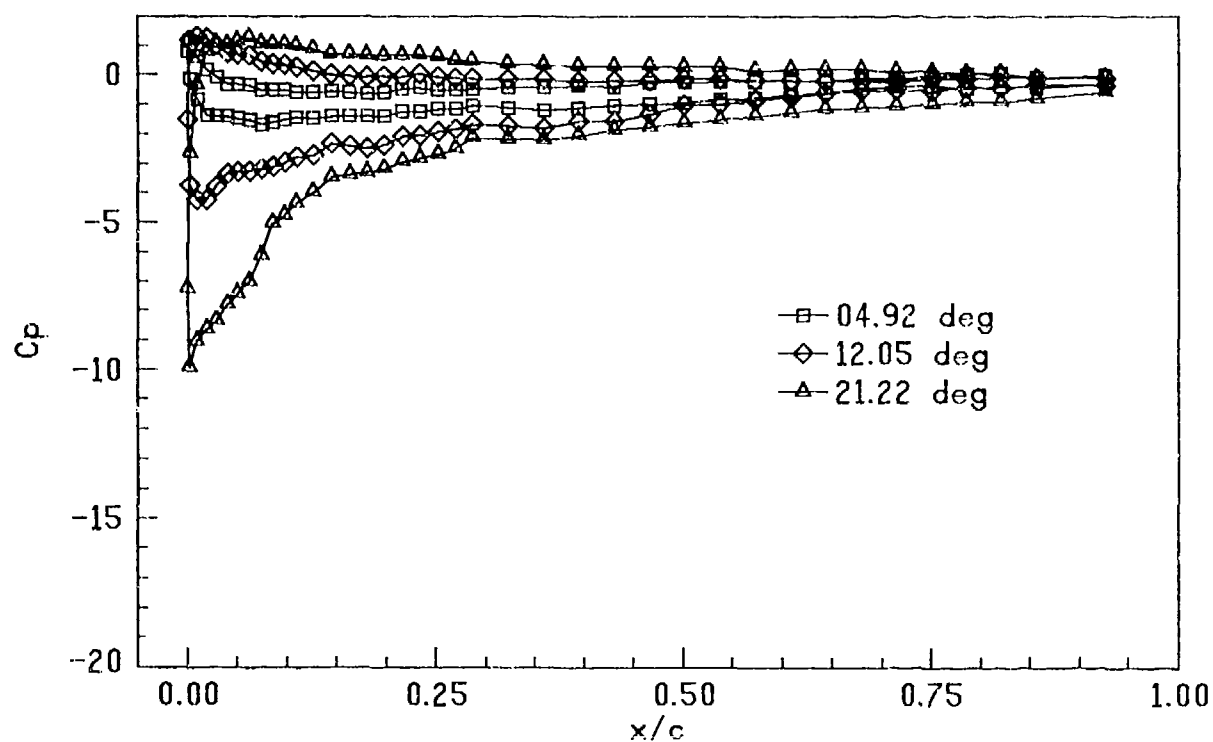
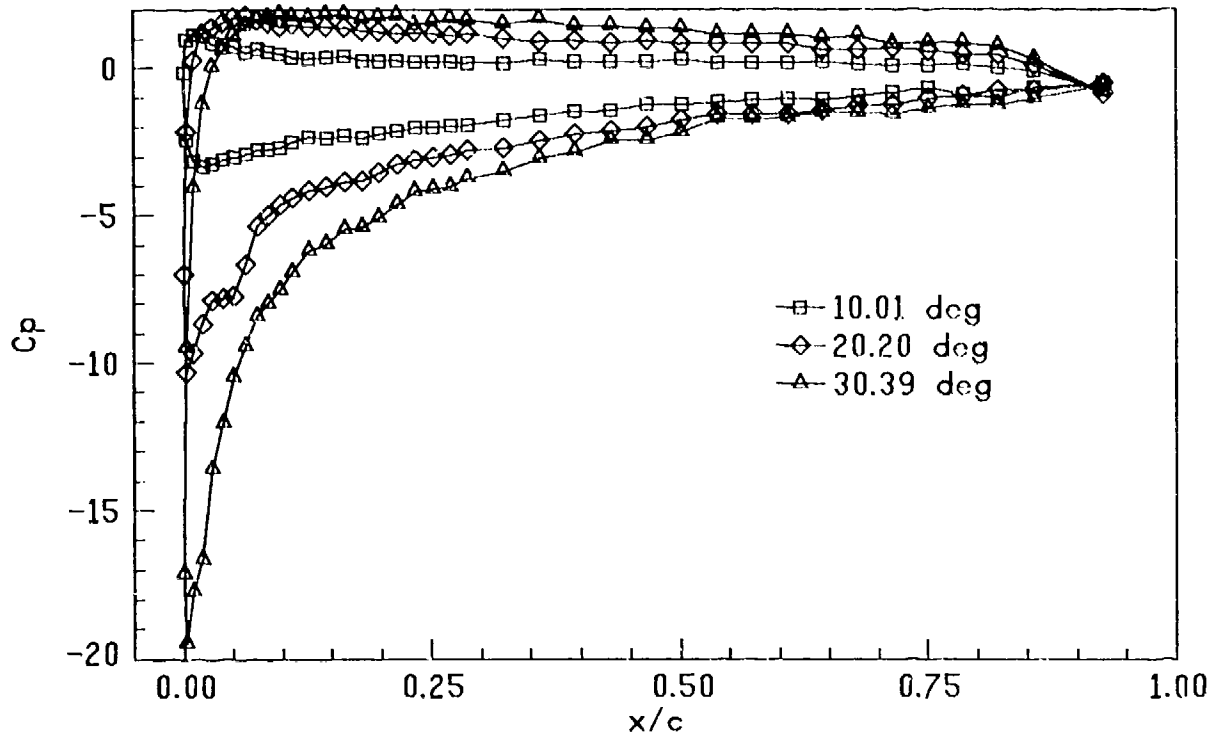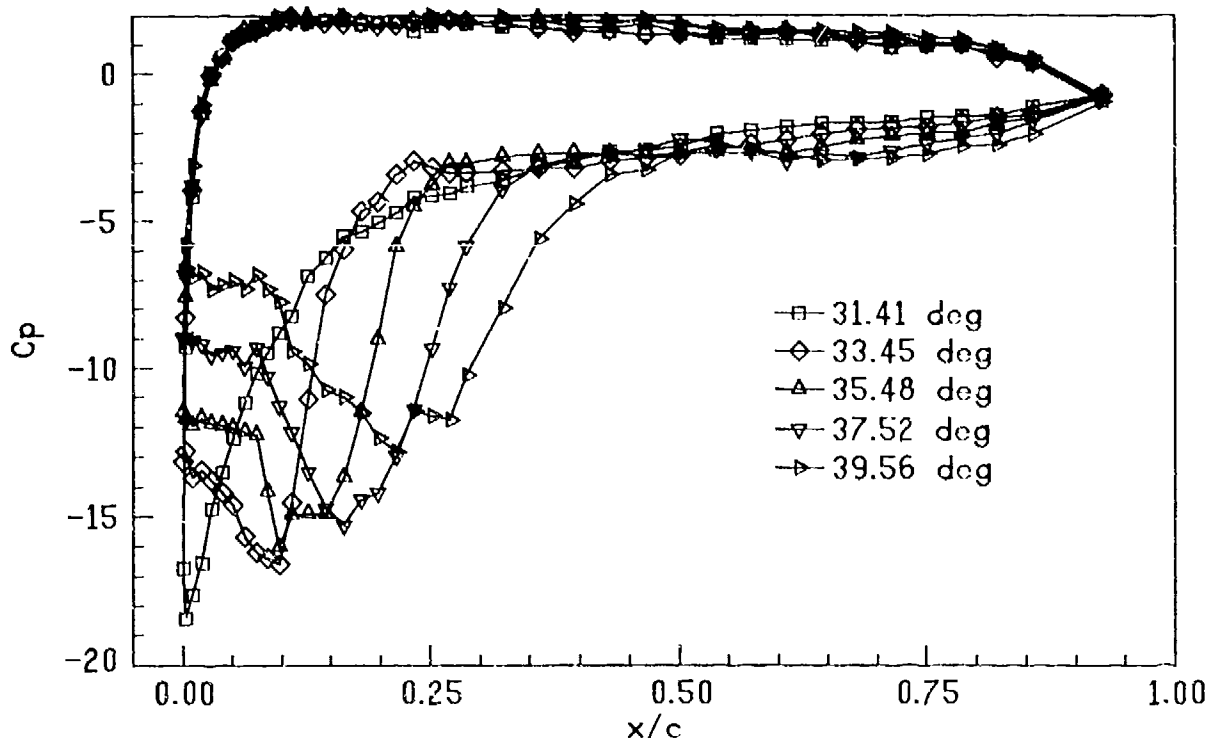Fig. 4a. Pressure distribution over the airfoil. $Re = 5.2 \times 10^1$; $a^+ = 0.072$
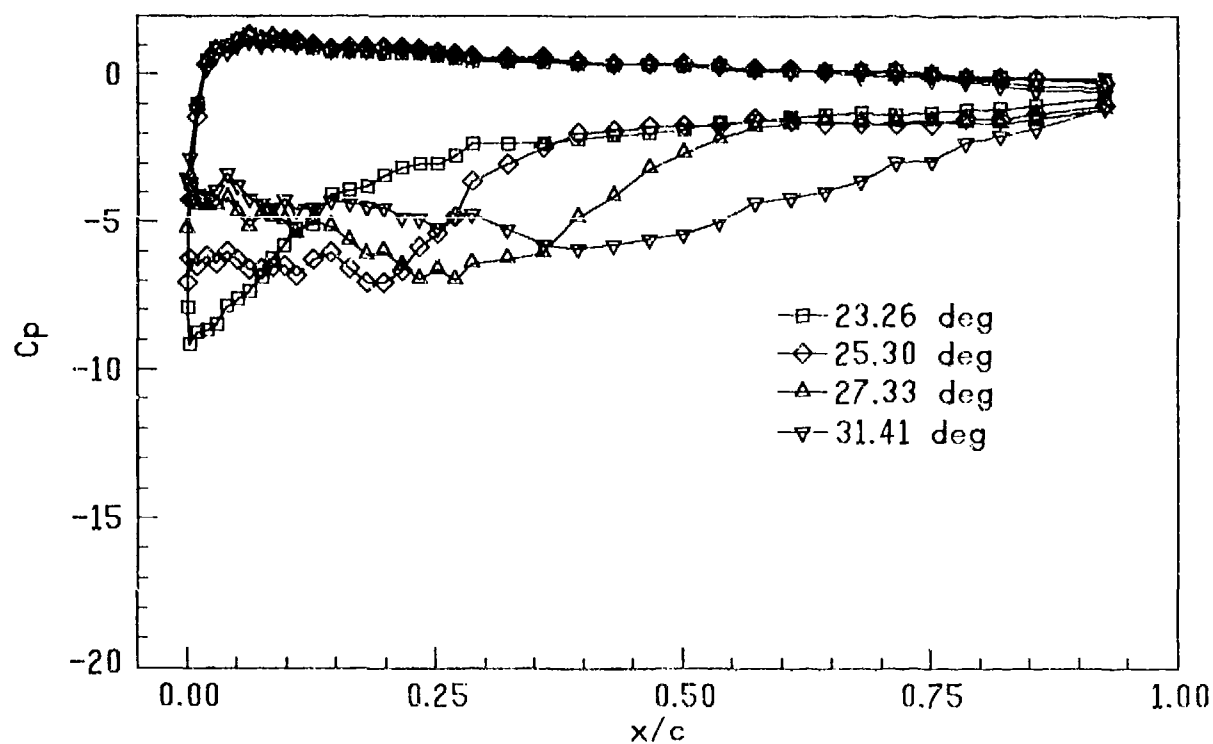
Fig. 4b. Pressure distribution over the airfoil. $Re = 5.2 \times 10^1$; $a^1 = 0.072$
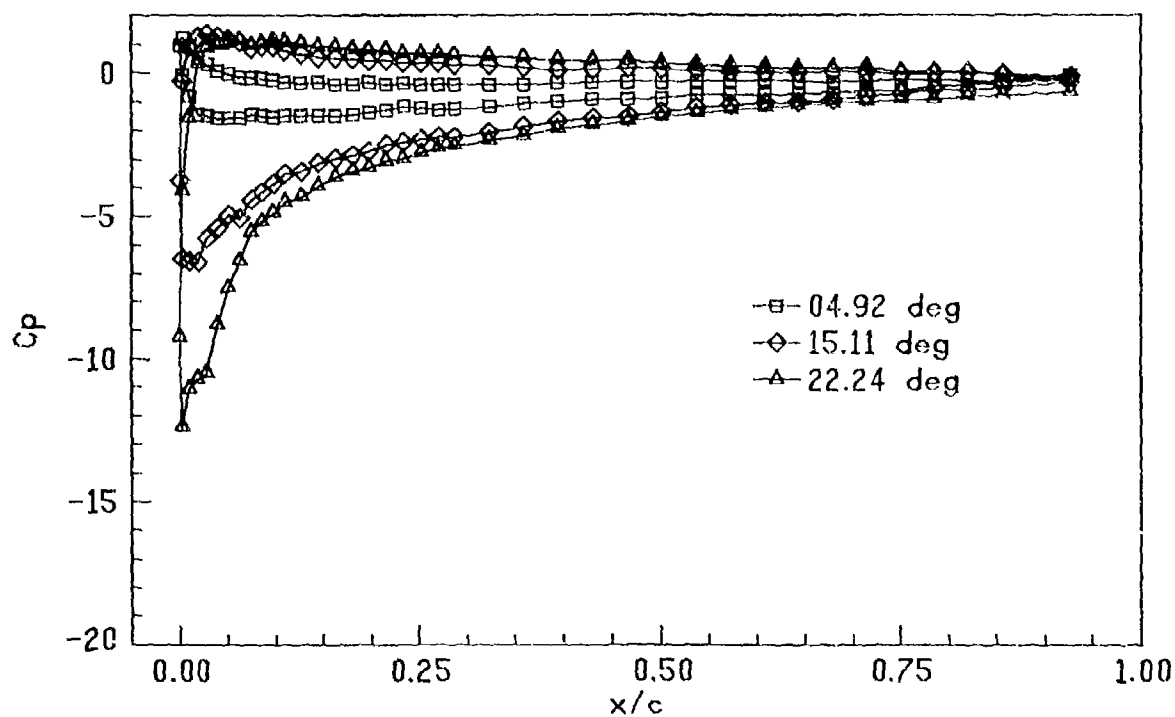
Fig. 5a. Pressure distribution over the airfoil. $Re = 1.4 \times 10^5$; $a^4 = 0.072$
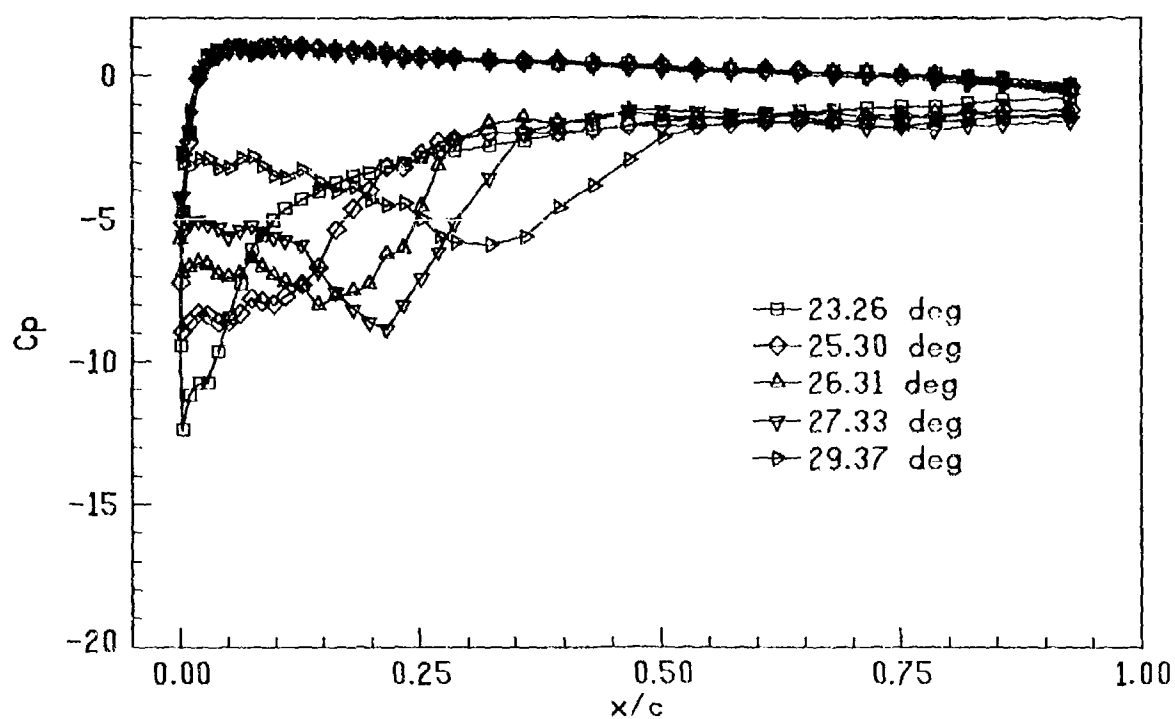
Fig. 5b. Pressure distribution over the airfoil. $Re = 1.4 \times 10^5$; $a^4 = 0.072$
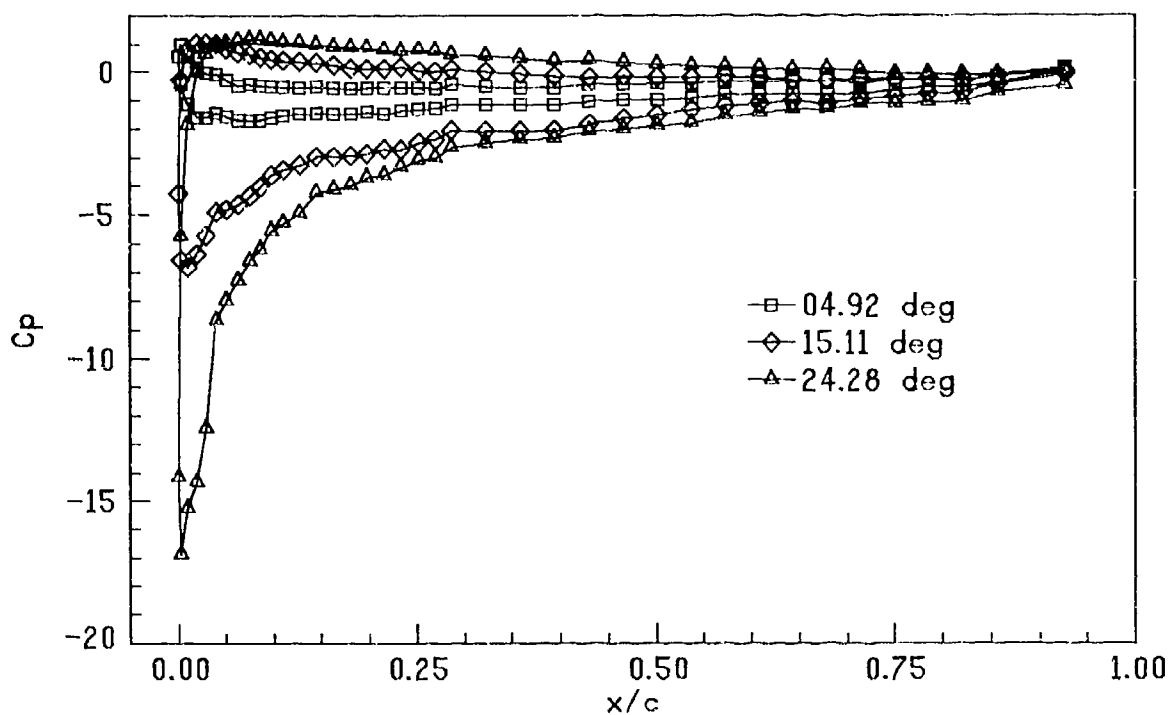
Fig. 6a. Pressure distribution over the airfoil. $Re = 2.2 \times 10^5$; $a^+ = 0.072$
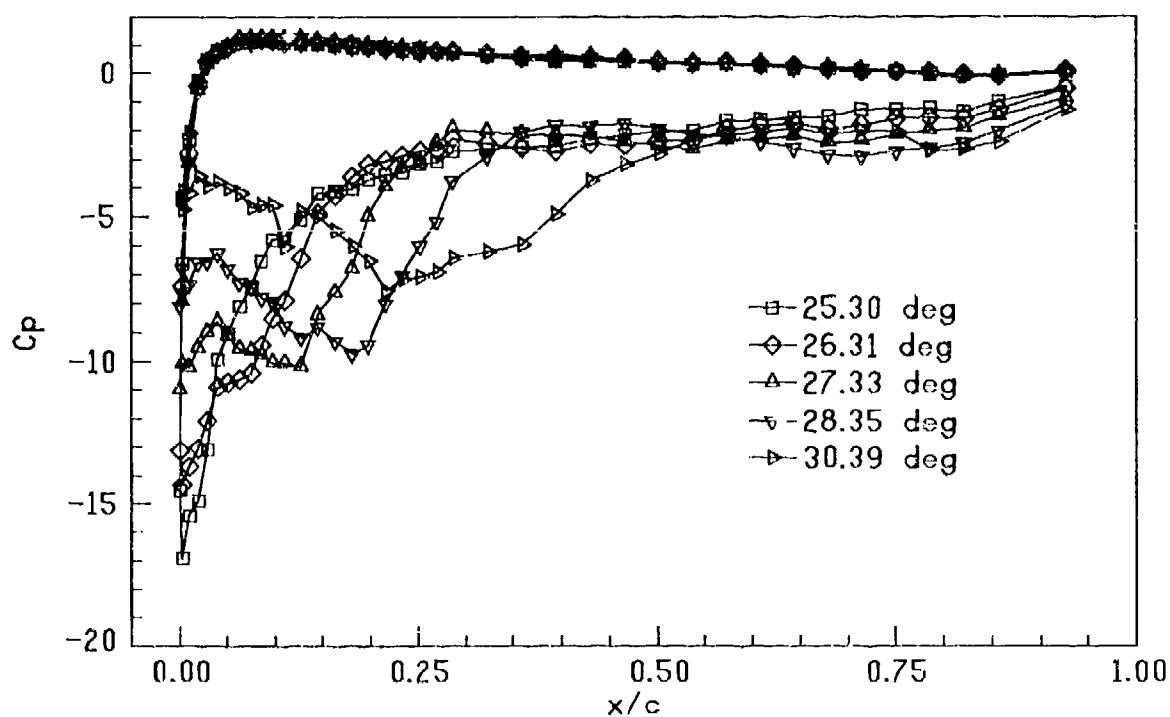
Fig. 6b. Pressure distribution over the airfoil. $Re = 2.2 \times 10^5$; $a^+ = 0.072$
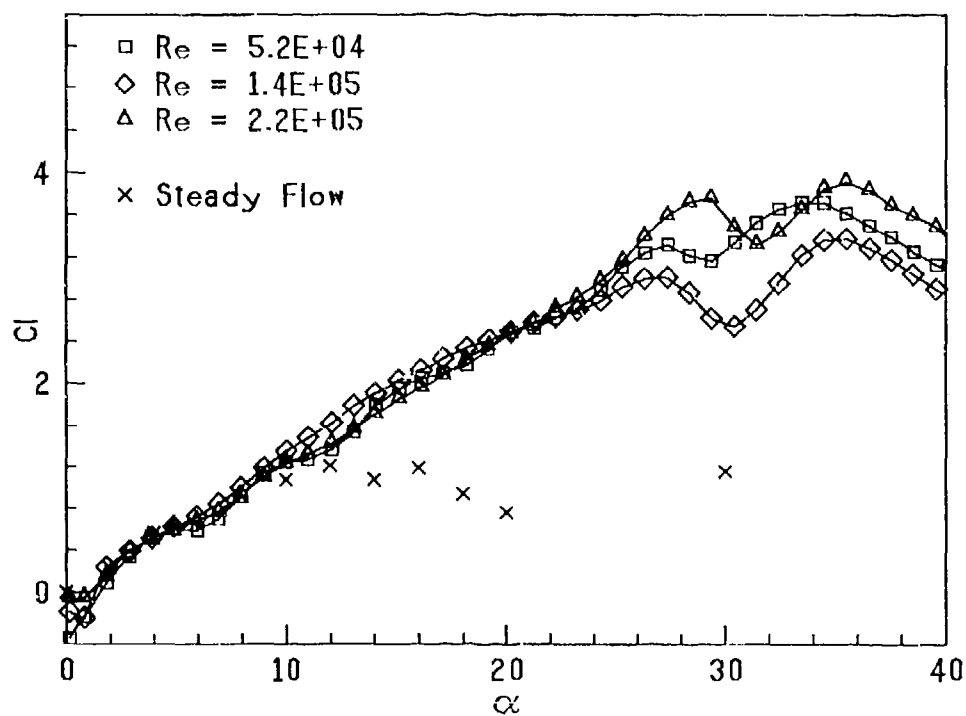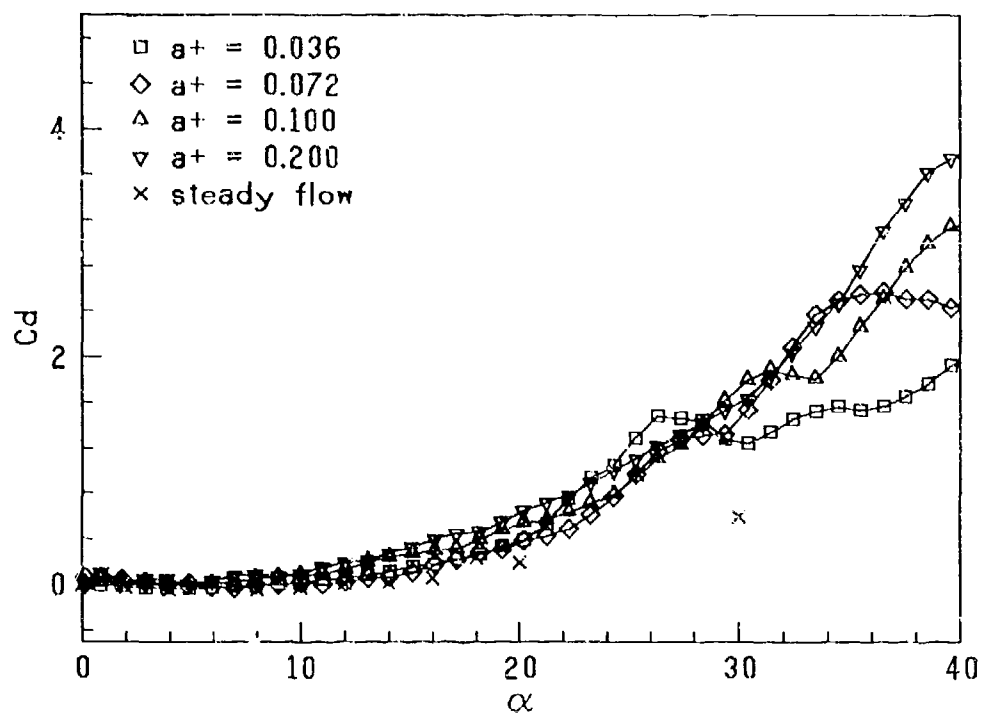
Fig. 7a. Variation of lift coefficient with Re. $a^+ = 0.072$
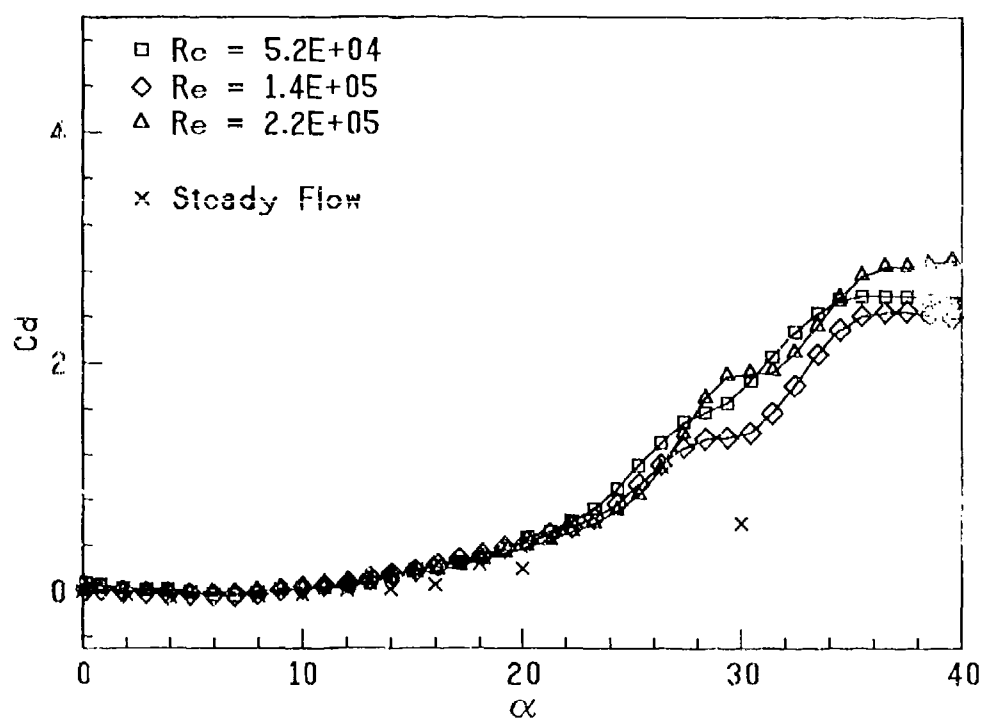
Fig. 7b. Variation of drag coefficient with Re. $a^+ = 0.072$
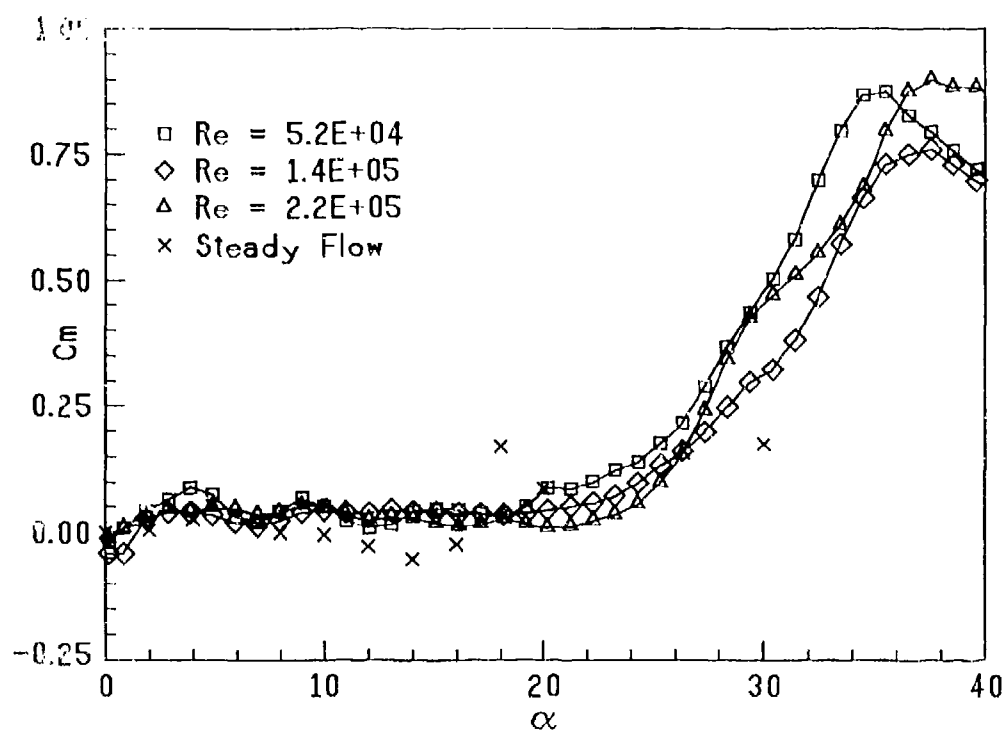
Fig. 7c. Variation of pitching moment coefficient with $\overline{Re}$. $\alpha^1 = 0.072$
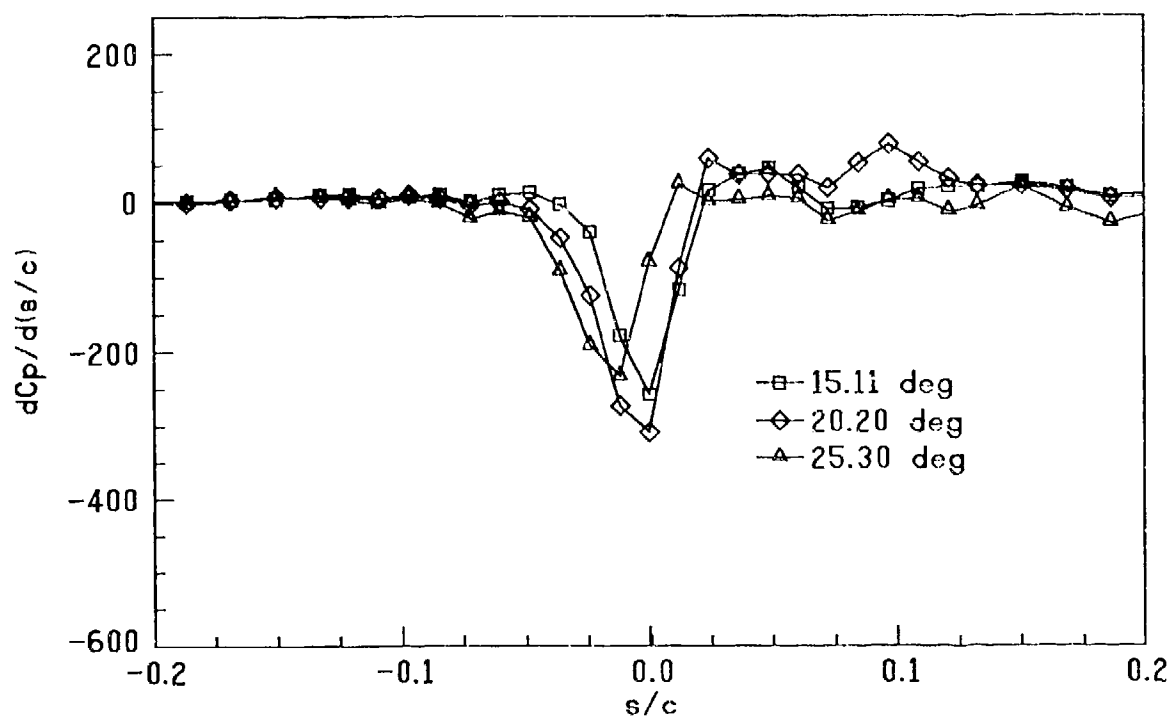
Fig. 8a. Pressure gradient distribution over the airfoil. $Re = 5.2 \times 10^4$; $a^+ = 0.072$
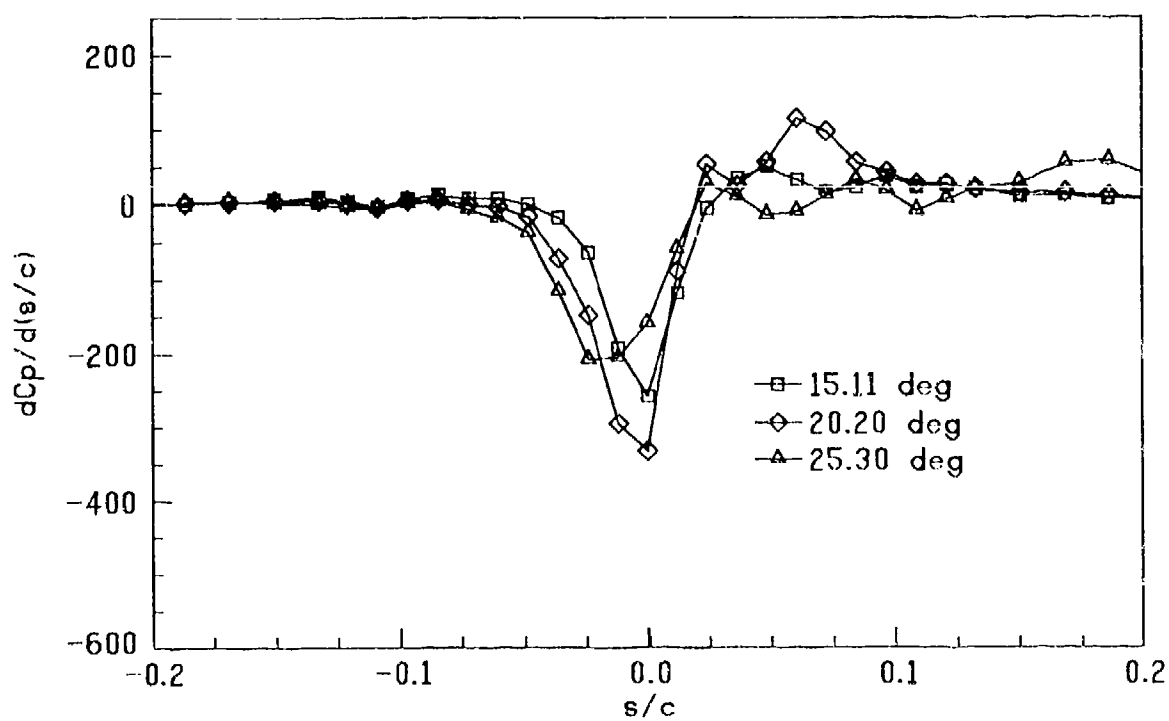
Fig. 8b. Pressure gradient distribution over the airfoil. $Re = 1.4 \times 10^5$; $a^+ = 0.072$
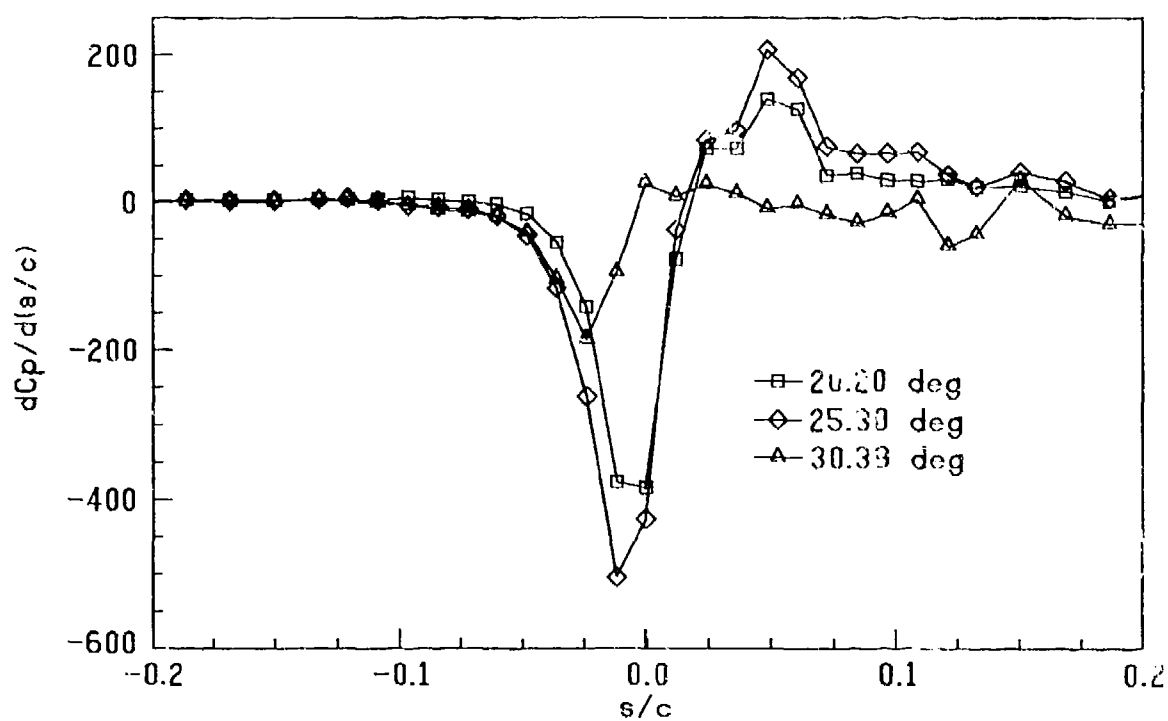
Fig. 8c. Pressure gradient distribution over the airfoil. $Re = 2.2 \times 10^5$; $a^+ = 0.072$
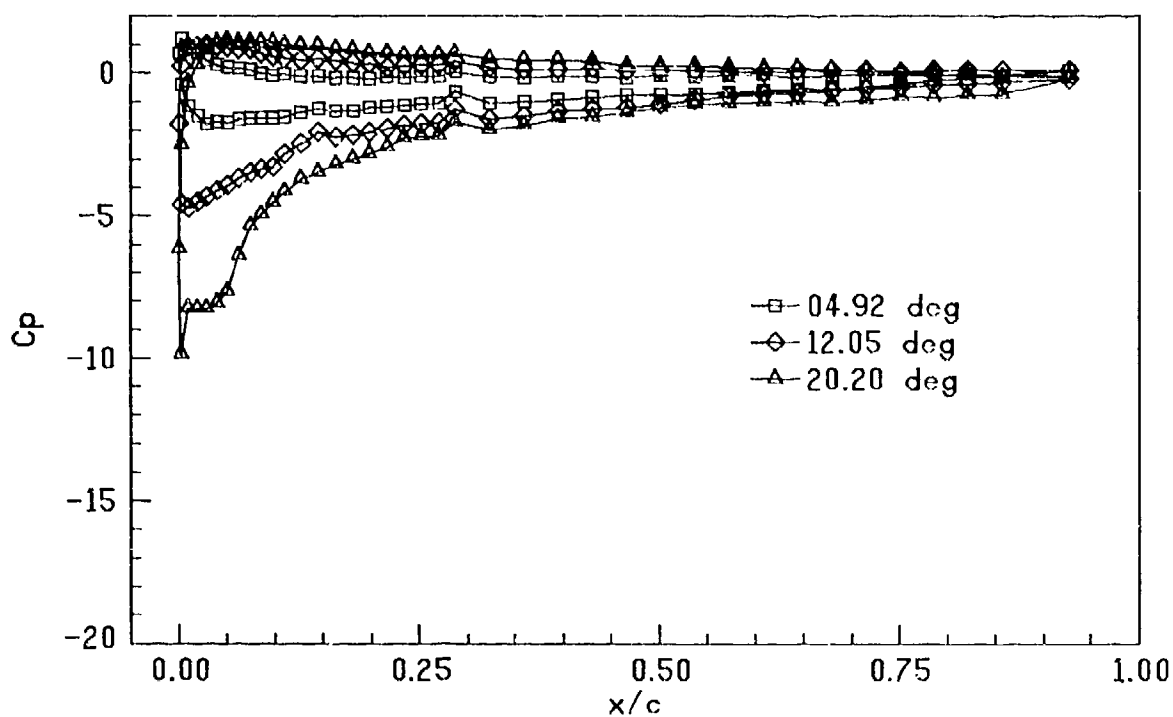
Fig. 9a. Pressure distribution over the airfoil. $Re = 1.3 \times 10^5$; $a^+ = 0.036$
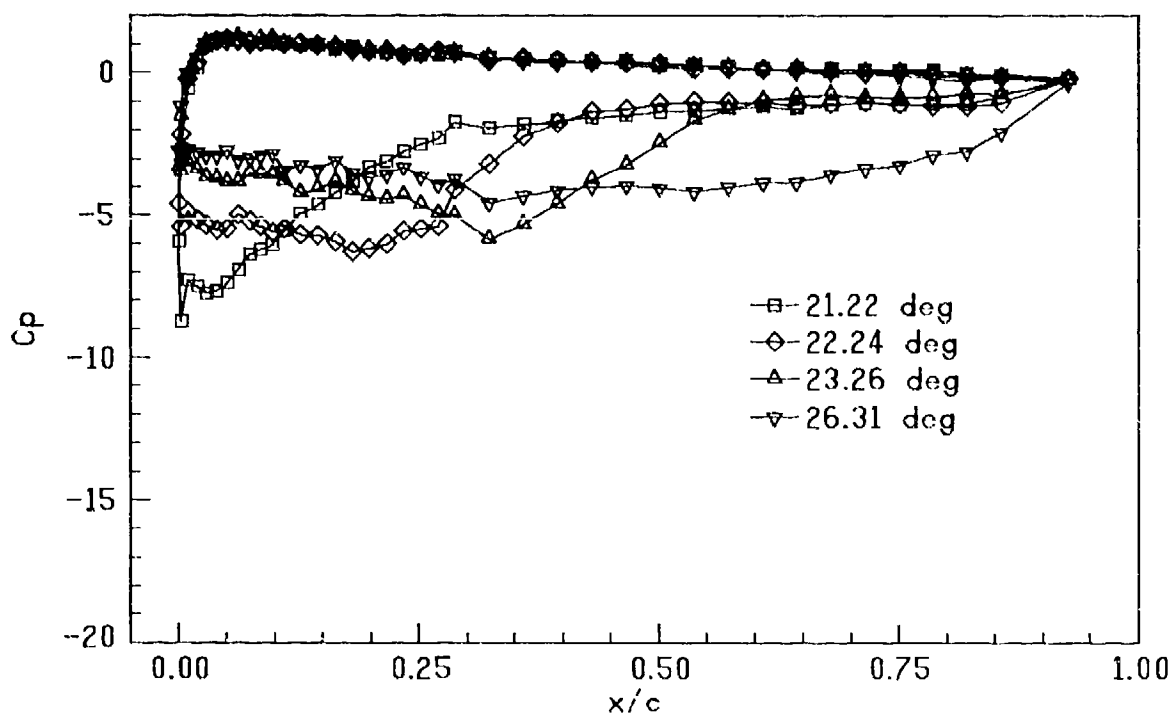
Fig. 9b. Pressure distribution over the airfoil. $Re = 1.3 \times 10^5$; $a^+ = 0.036$
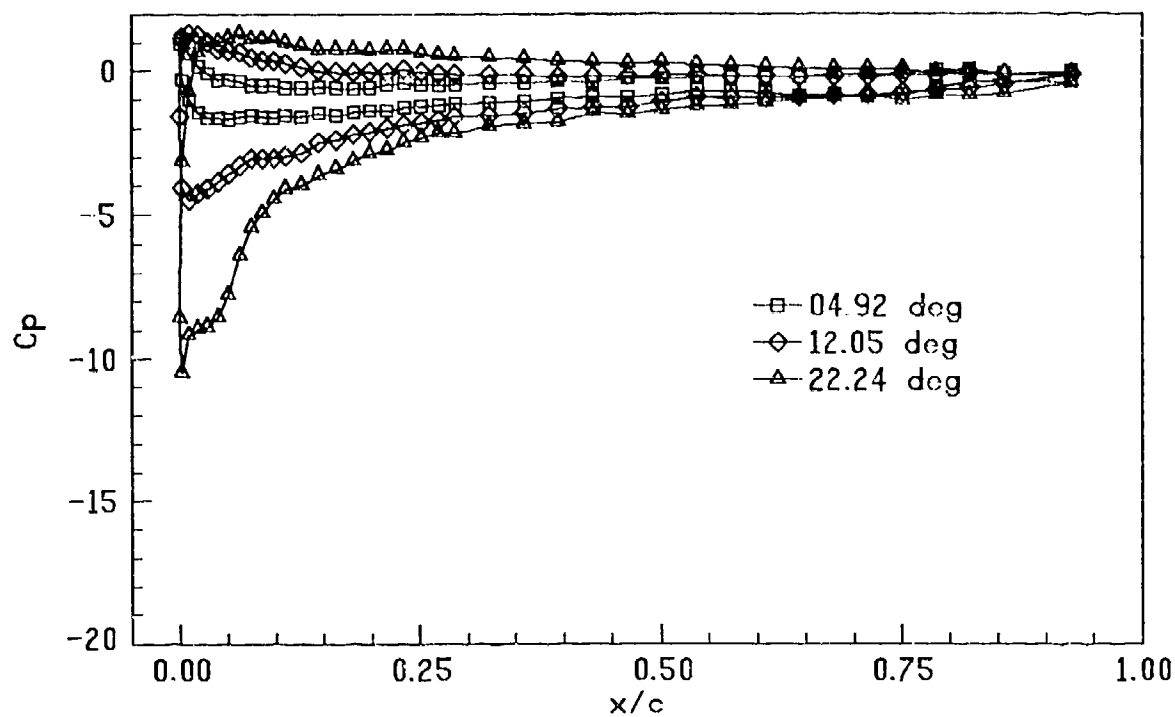
Fig. 10a. Pressure distribution over the airfoil. $Re = 1.2 \times 10^5$; $a^+ = 0.072$
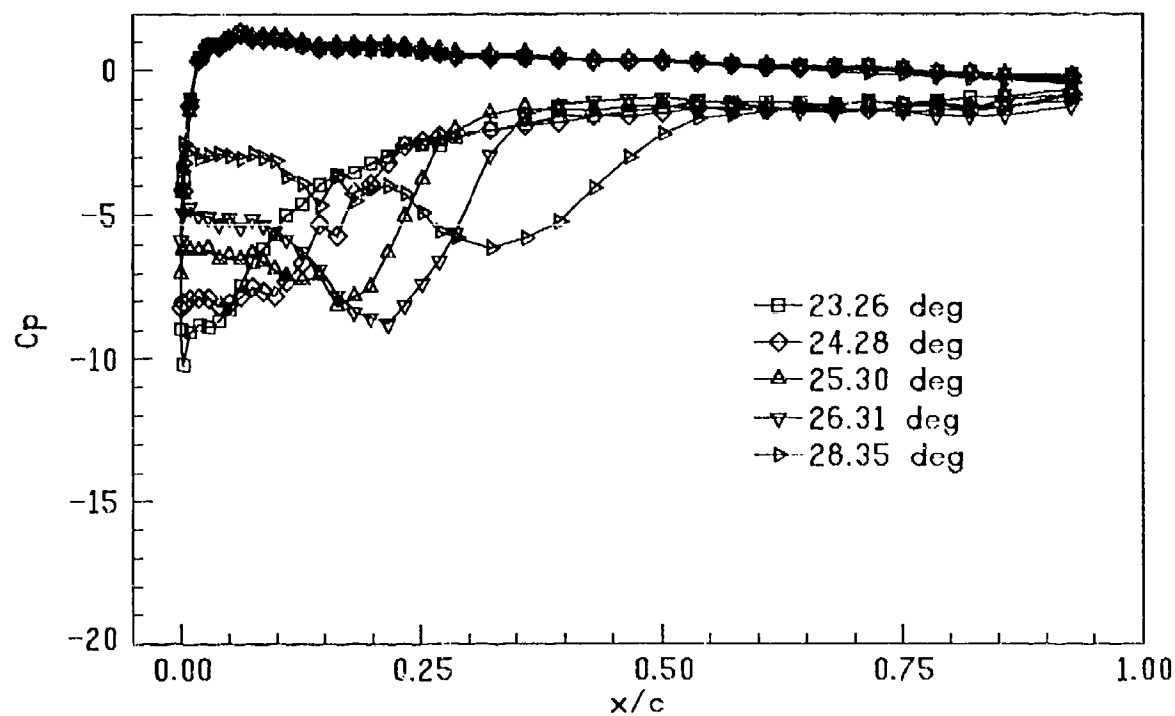
Fig. 10b. Pressure distribution over the airfoil. $Re = 1.2 \times 10^5$; $a^+ = 0.072$
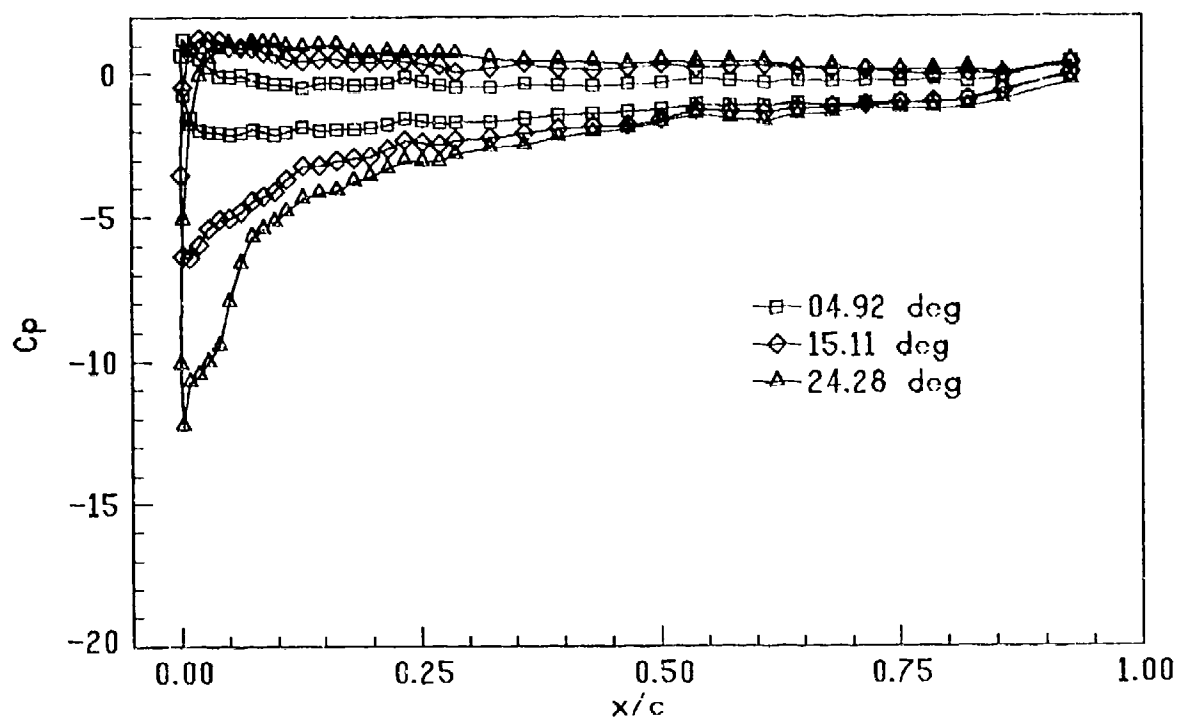
Fig. 11a. Pressure distribution over the airfoil. $Re = 1.3 \times 10^5$; $a^+ = 0.100$
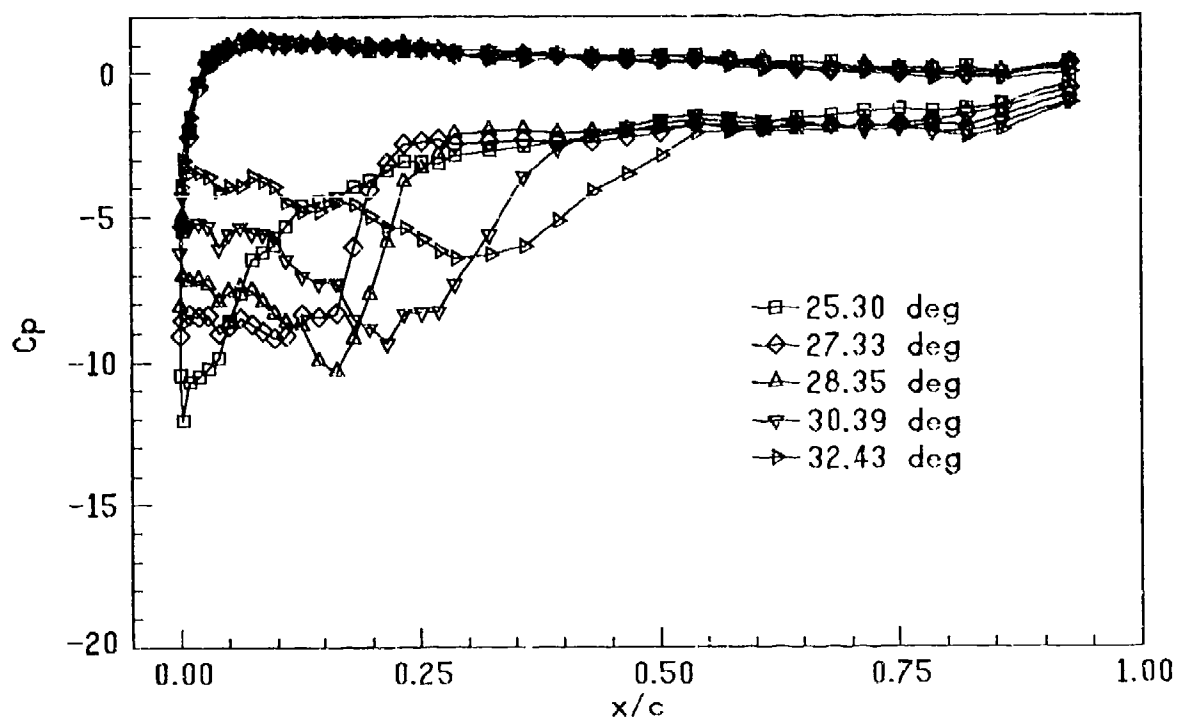
Fig. 11b. Pressure distribution over the airfoil. $Re = 1.3 \times 10^5$; $a^+ = 0.100$

Fig. 12a. Pressure distribution over the airfoil. $Re = 1.2 \times 10^5$; $a^+ = 0.200$

Fig. 12b. Pressure distribution over the airfoil. $Re = 1.2 \times 10^5$; $a^+ = 0.200$
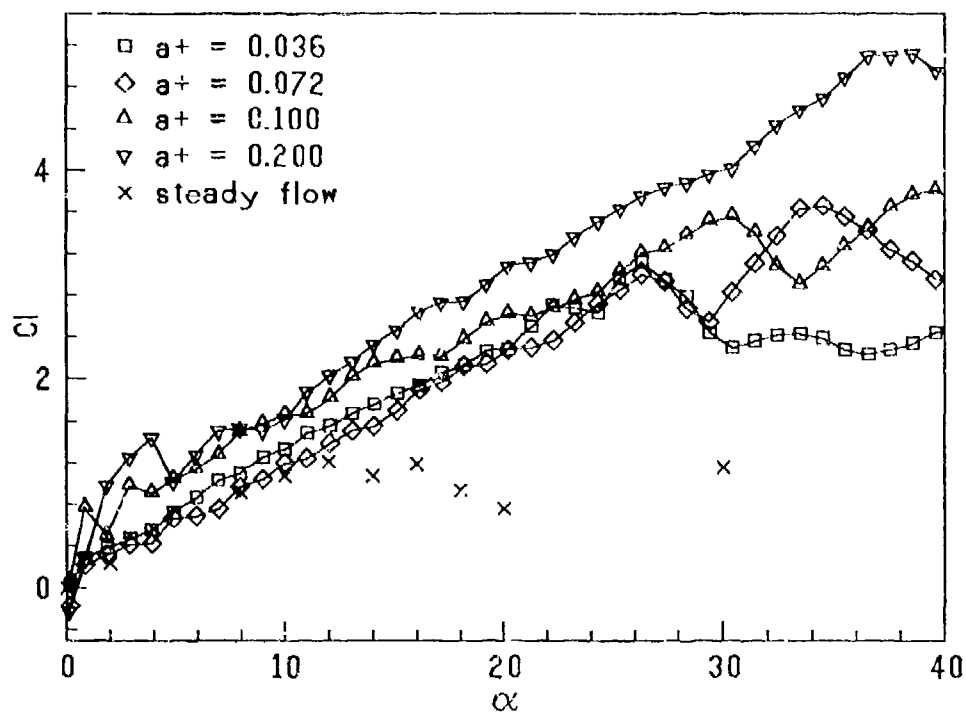
Fig. 13a. Variation of lift coefficient with a^1. $Re \approx 1.3 \times 10^5$

Fig. 13b. Variation of drag coefficient with a^1. $Re \approx 1.3 \times 10^5$

Fig. 13c. Variation of pitching moment coefficient with a^+. $Re \approx 1.3 \times 10^5$
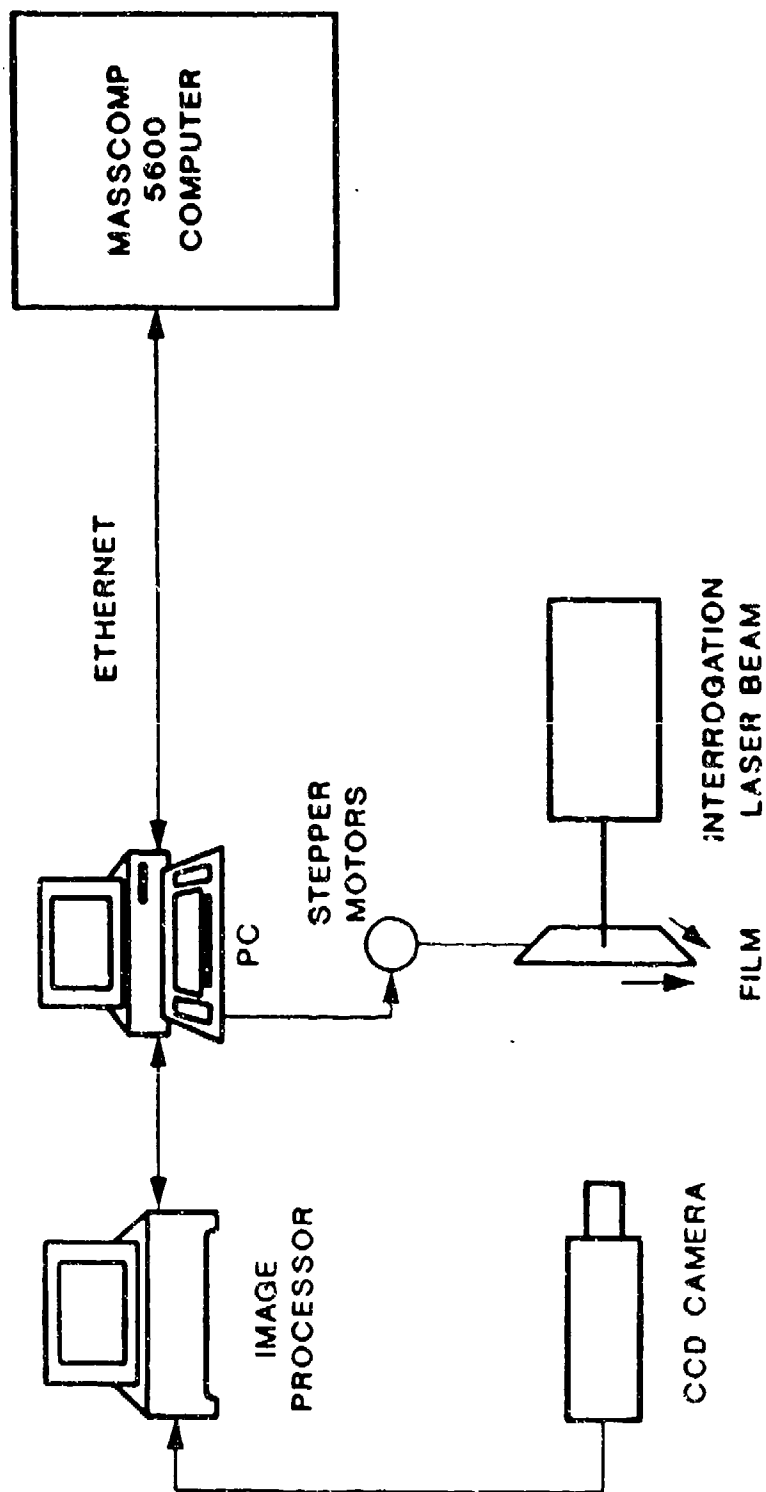
Fig. 14. Schematic of the PIV system
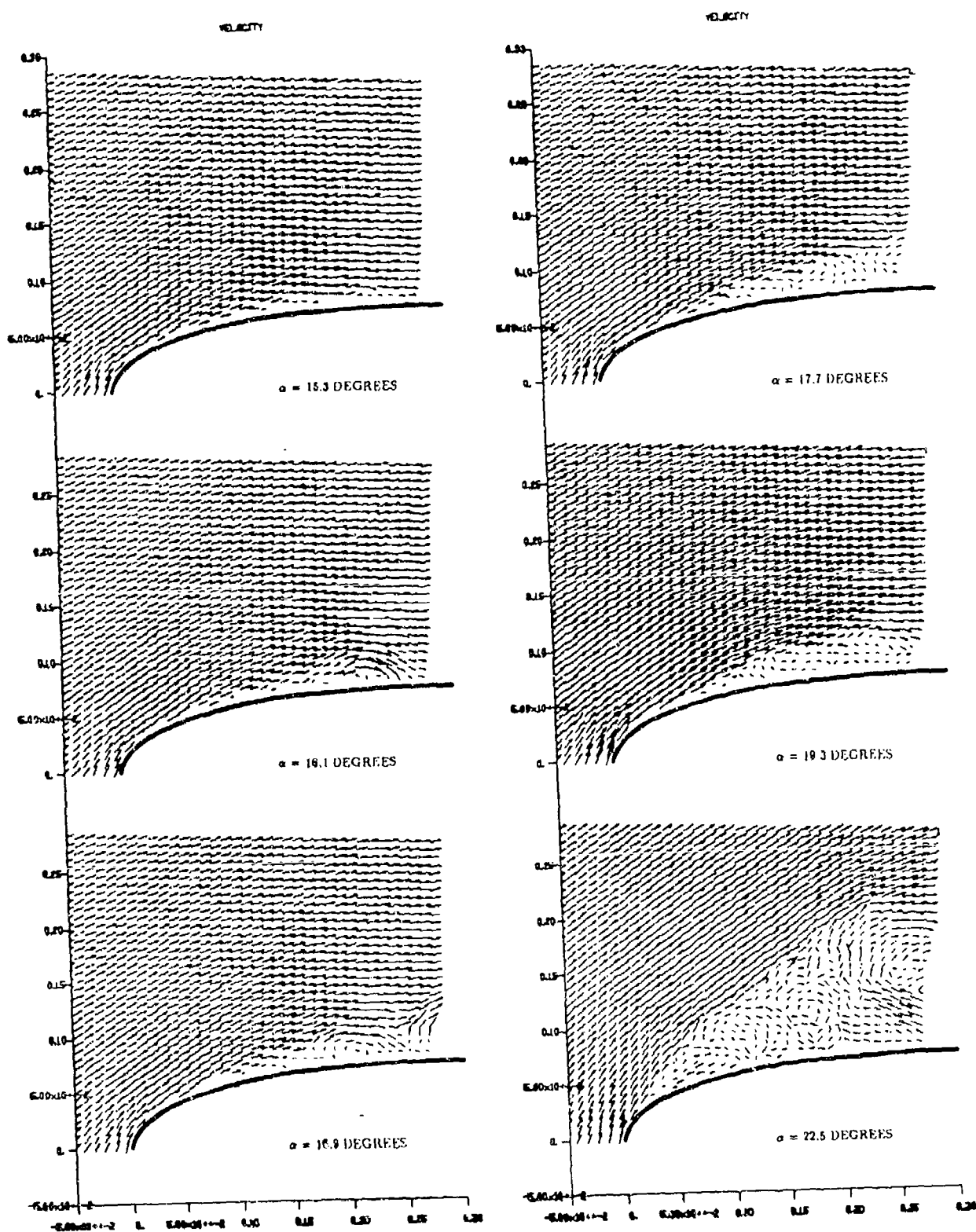
Fig. 15. Velocity vectors in the leading-edge region of the airfoil

Fig. 16. Vorticity field in the leading-edge region of the airfoil
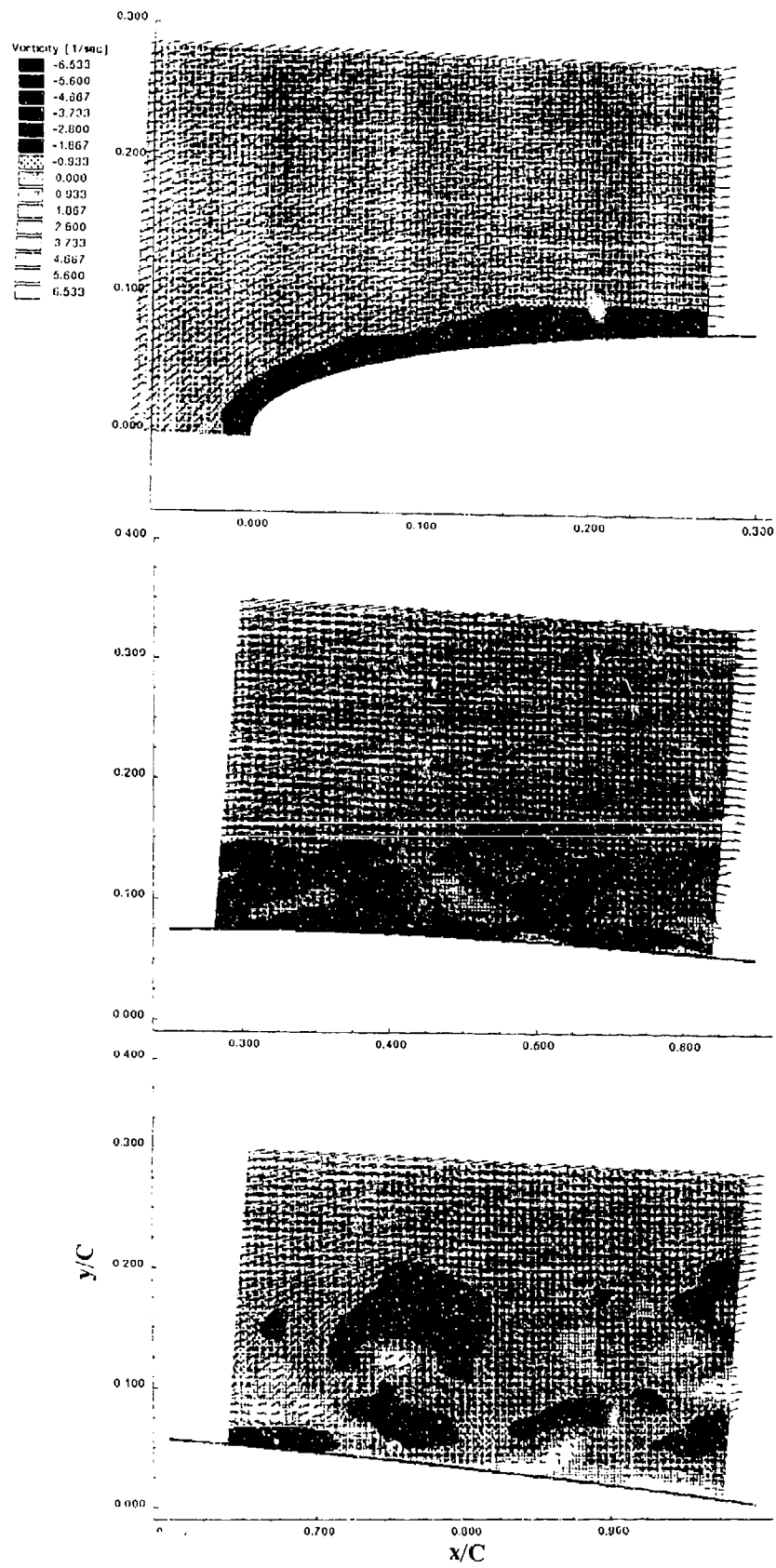
Fig. 17. Velocity and vorticity fields in the front, mid and aft sections at $\alpha = 15.3$ degrees
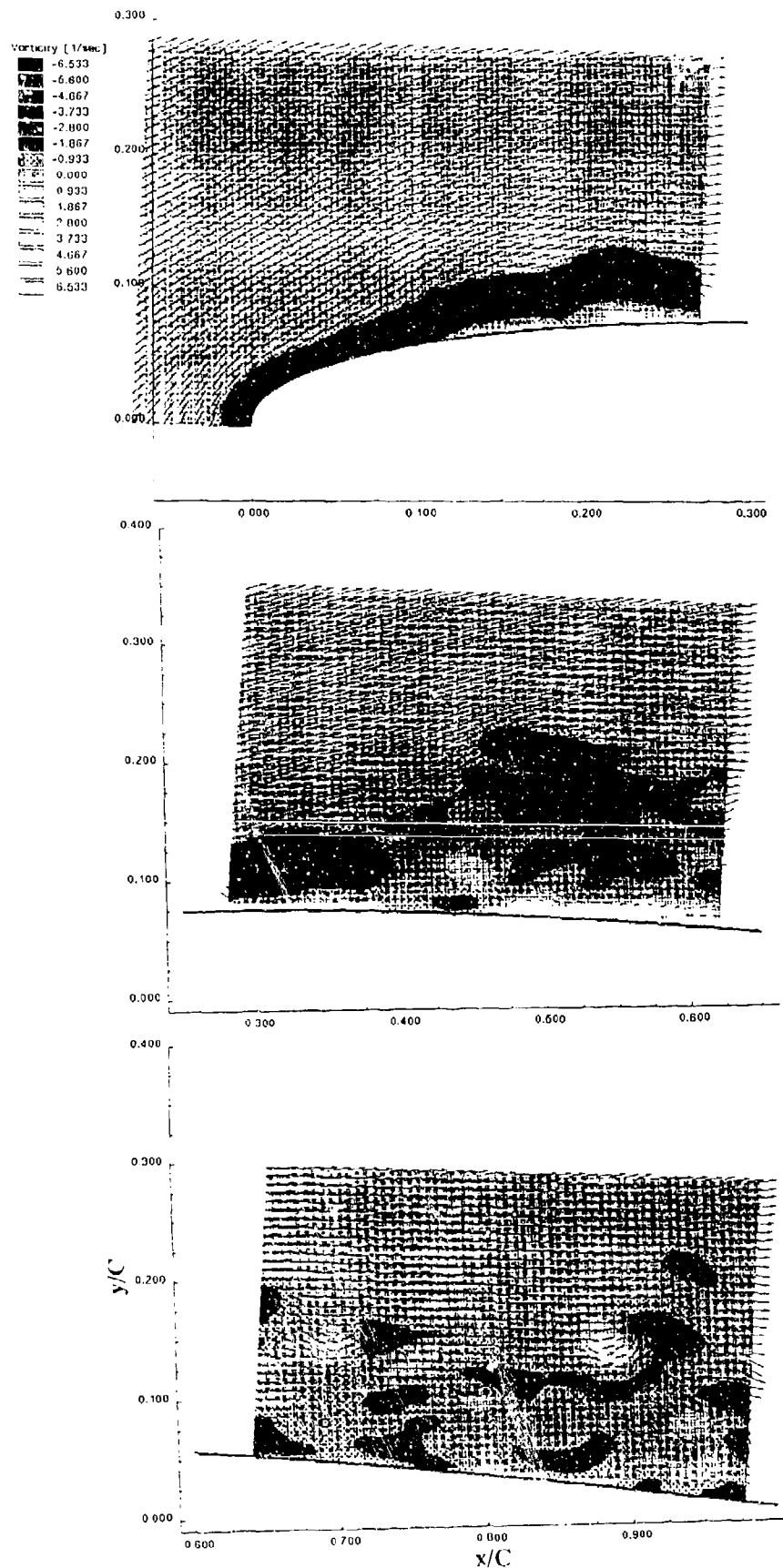
Fig. 18. Velocity and vorticity fields in the front, mid and aft sections at
α = 20.1 degrees
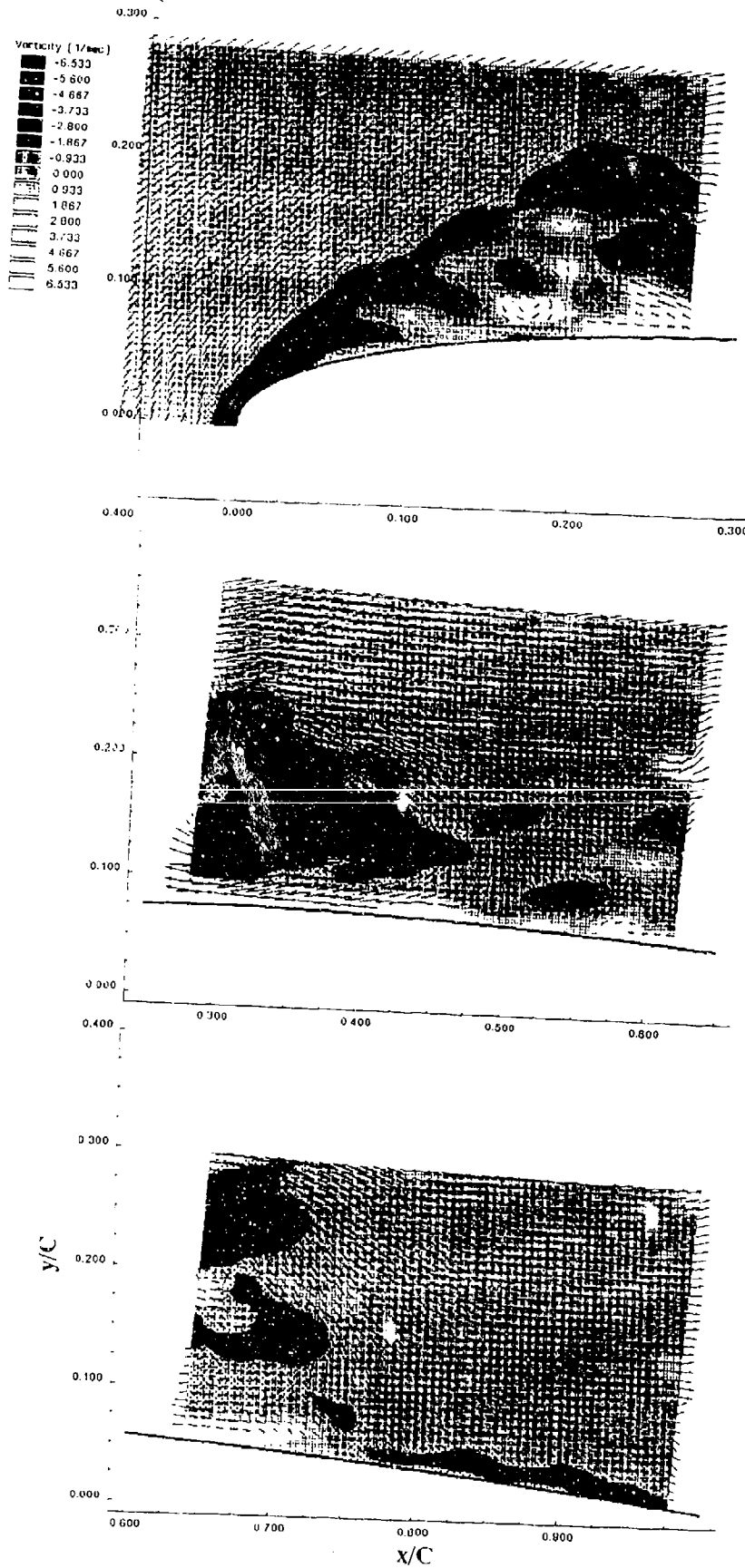
Fig. 19. Velocity and vorticity fields in the front, mid and aft sections at $\alpha = 23.4$ degrees
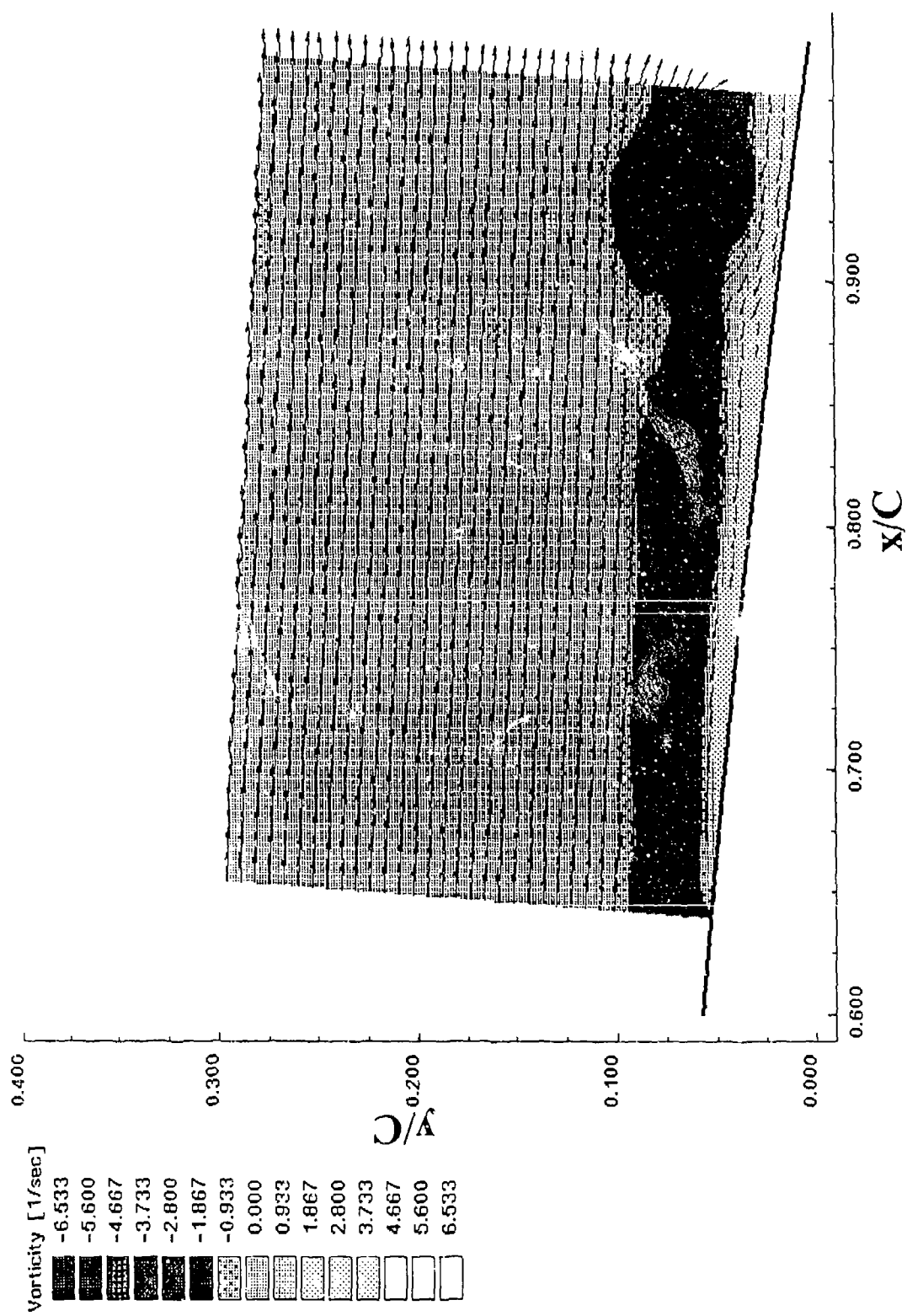
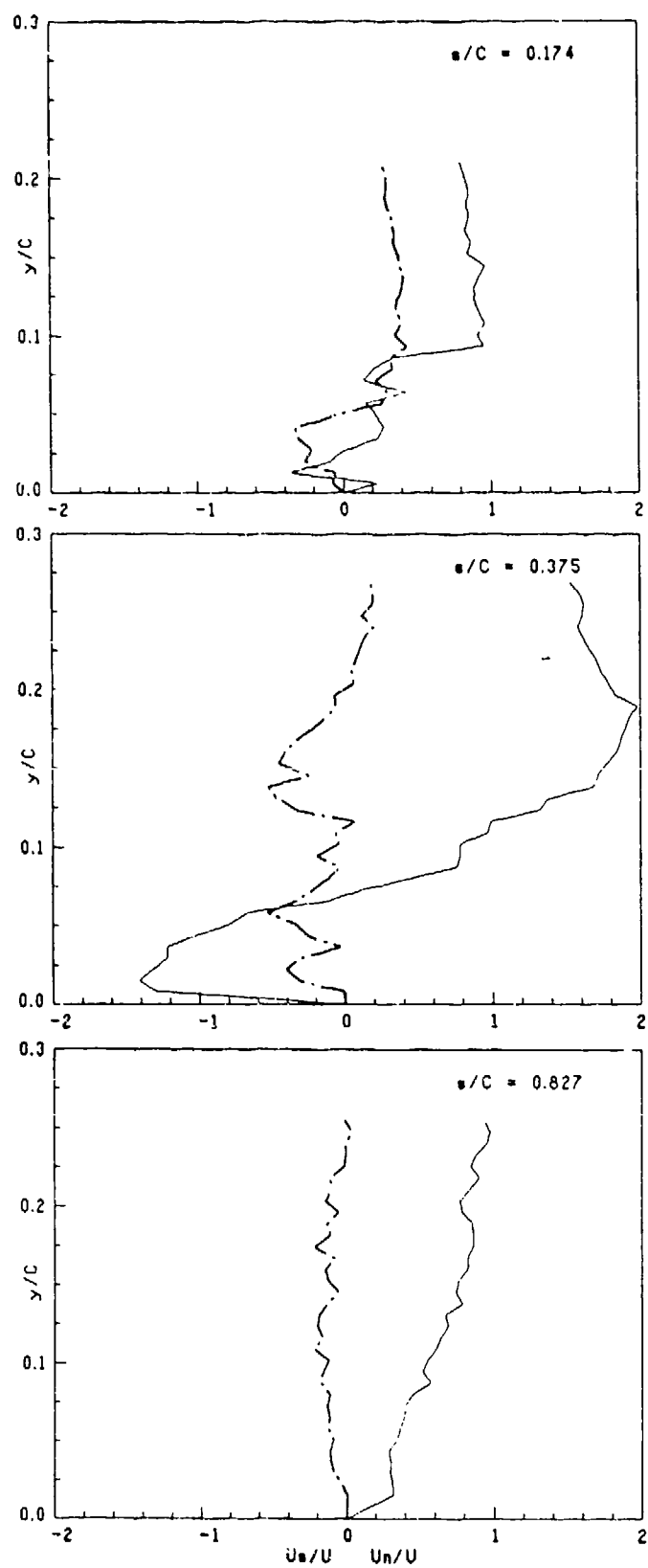Fig. 20. Velocity and vorticity fields in the trailing region of the airfoil at
$\alpha = 8.9$ degrees
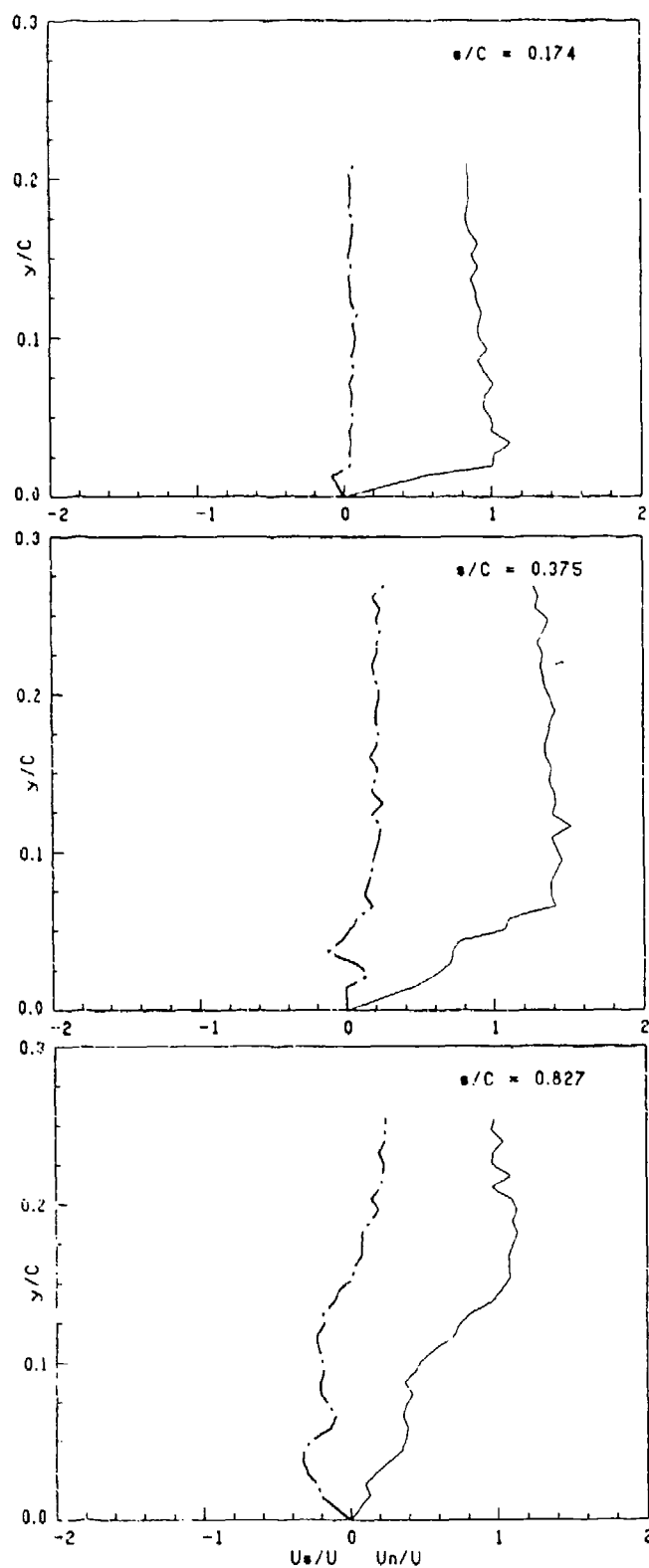
Fig. 21. Typical velocity distributions at different longitudinal locations
$\alpha = 15.3$ degrees; ——U_s/U; —·—U_n/U
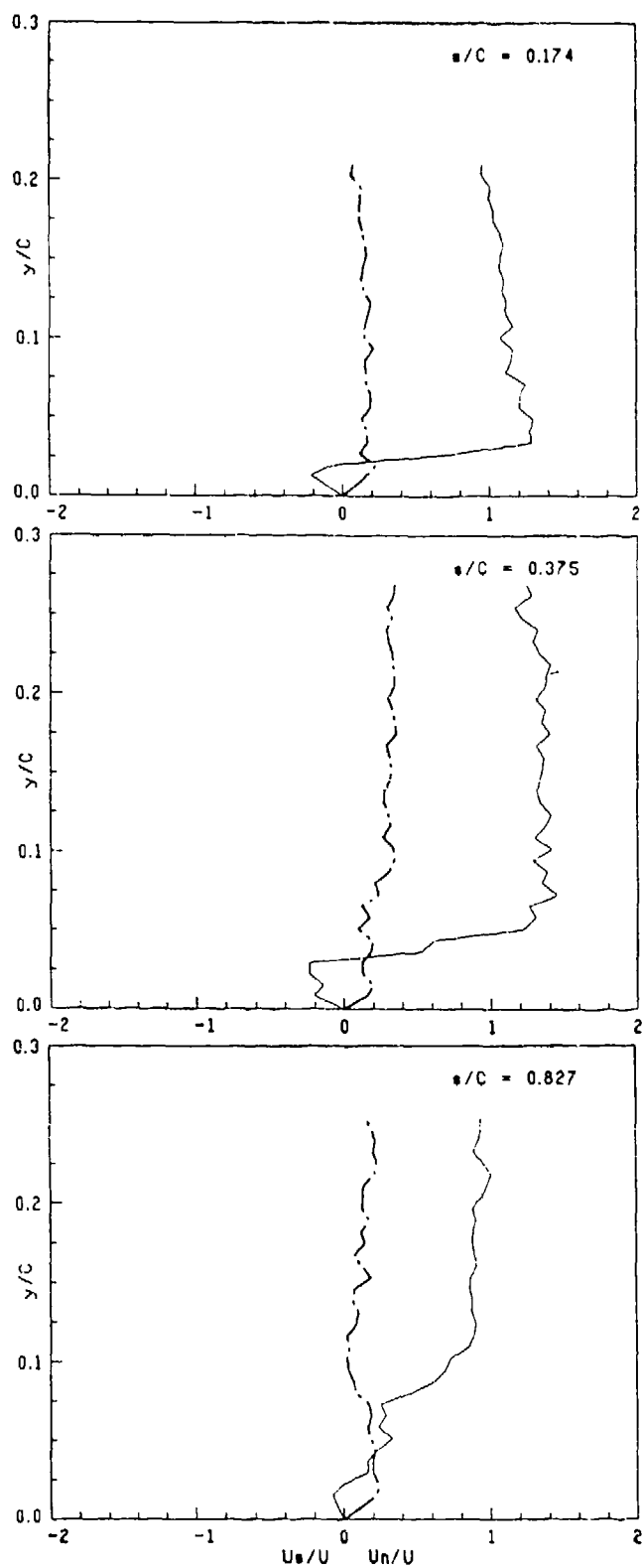
Fig. 22. Typical velocity distributions at different longitudinal locations
$\alpha = 20.1$ degrees; ——U_s/U; ———U_n/U

Fig. 23. Typical velocity distributions at different longitudinal locations
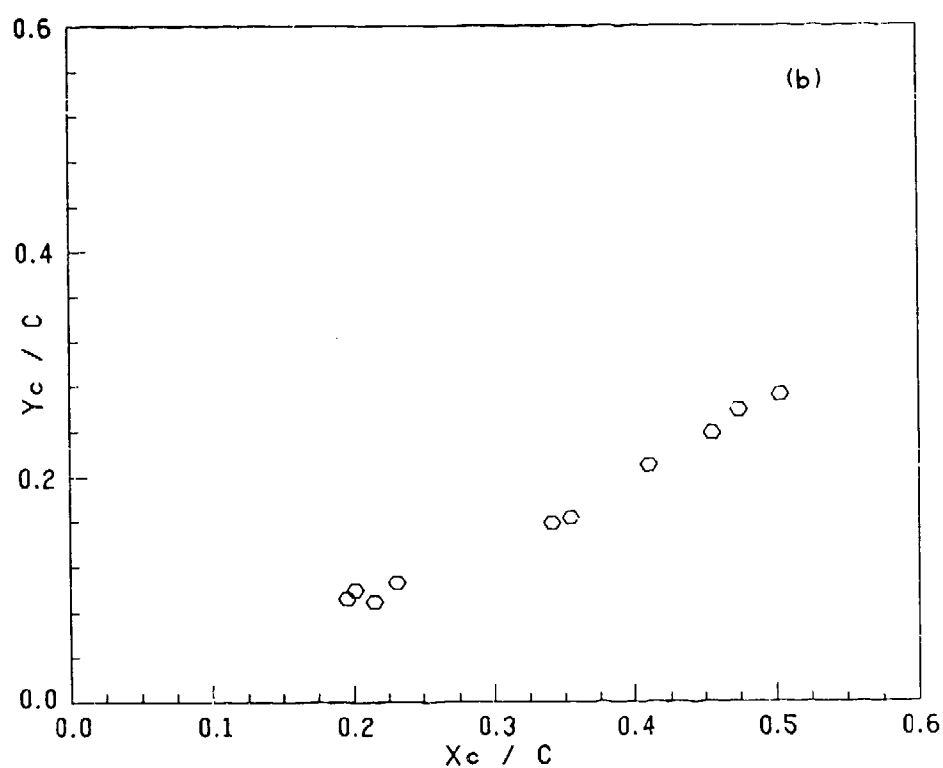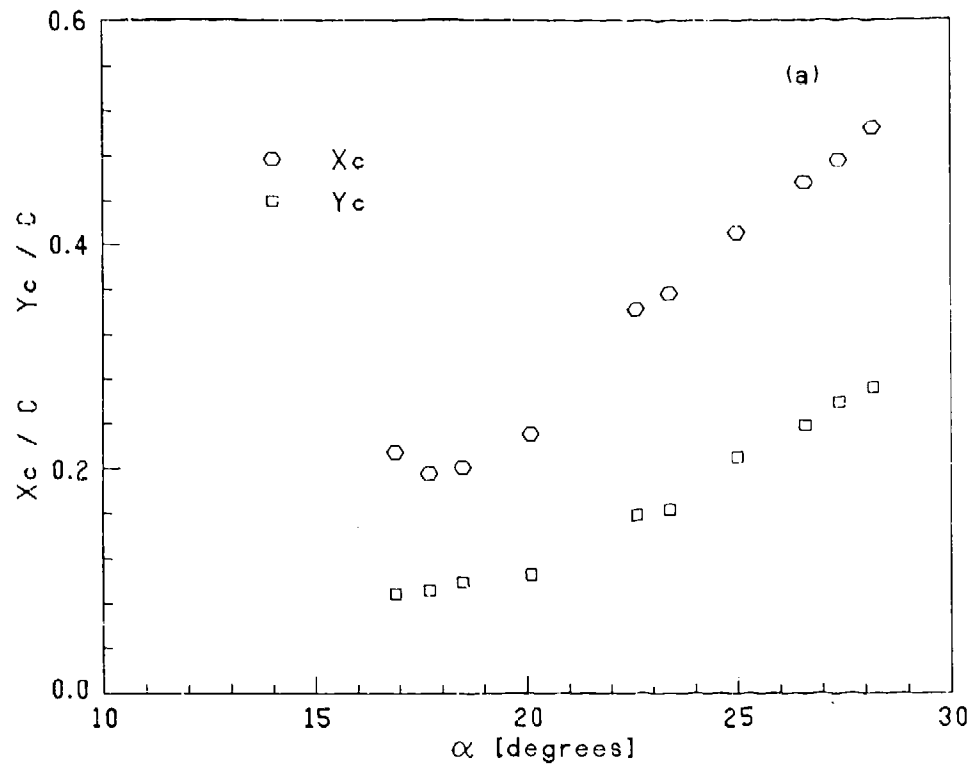$\alpha = 23.4$ degrees; —— U_s/U; —·—U_n/U

Fig. 24. (a) The longitudinal and cross-stream displacements of the dynamic stall vortex center during the pitching process. (b) The trajectory of the dynamic-stall vortex center during pitching
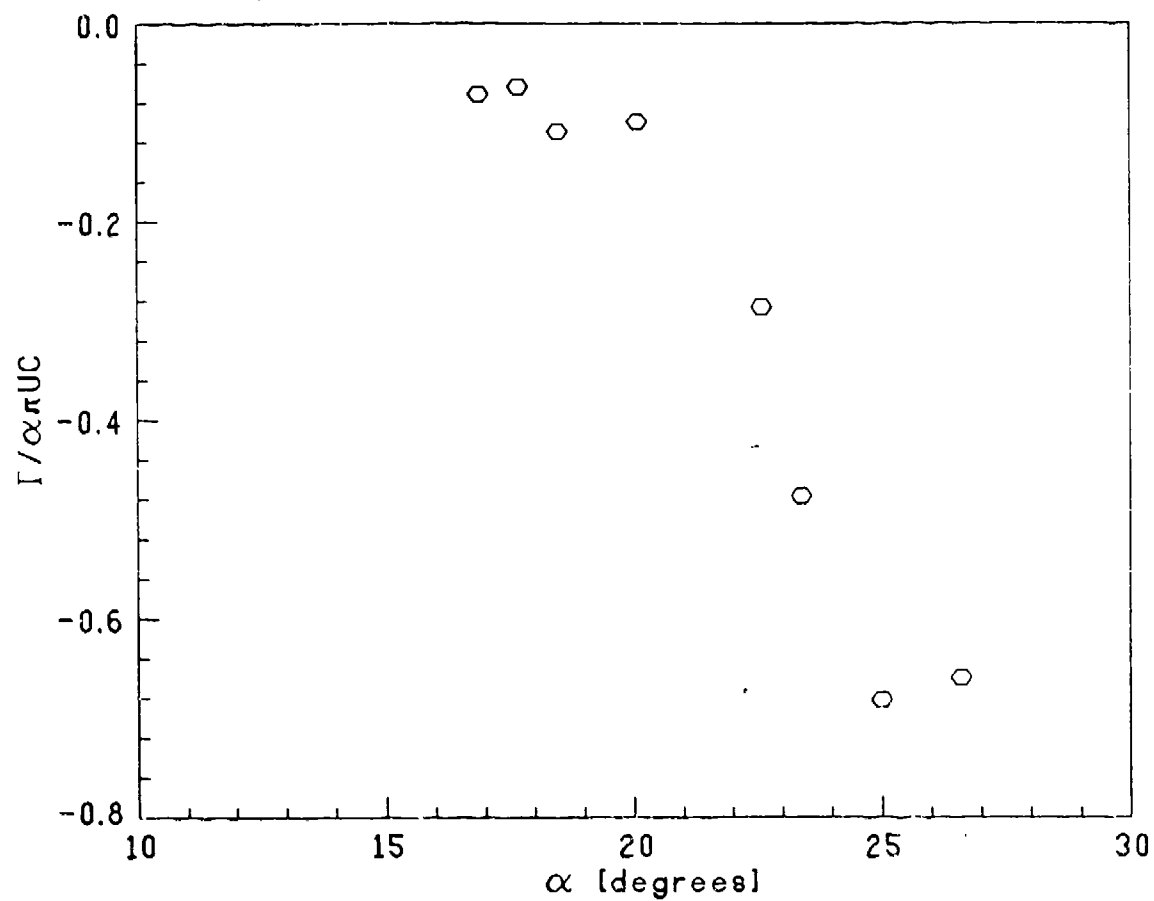
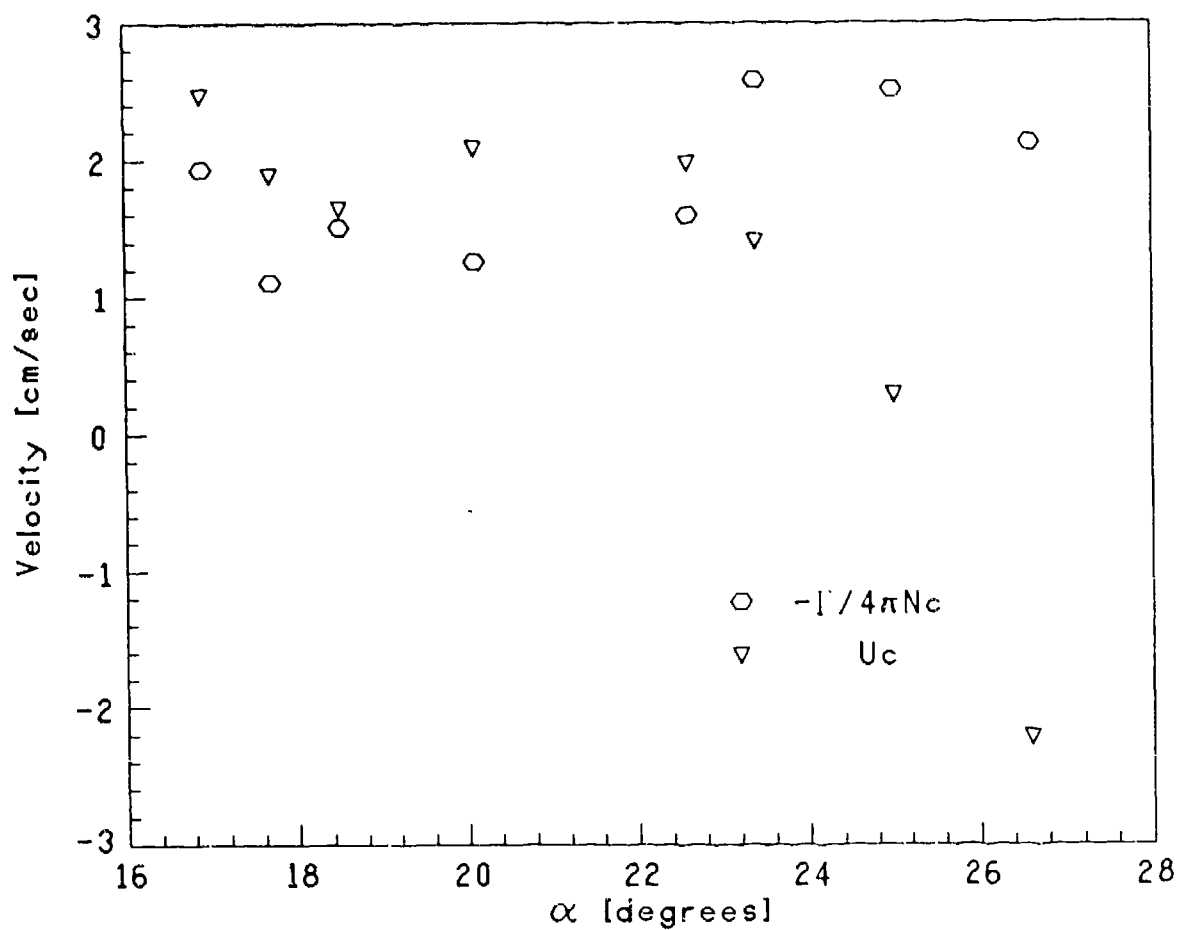Fig. 25. Circulation associated with dynamic-stall vortex center during pitching

Fig. 26. Verification of the image vortex model for the dynamic-stall vortex